12-2015

Border-Collision Bifurcations of Cardiac Calcium Cycling

Jacob Michael Kahle
University of Tennessee - Knoxville, jkahle@vols.utk.edu

To the Graduate Council:

I am submitting herewith a thesis written by Jacob Michael Kahle entitled "Border-Collision Bifurcations of Cardiac Calcium Cycling." I have examined the final electronic copy of this thesis for form and content and recommend that it be accepted in partial fulfillment of the requirements for the degree of Master of Science, with a major in Mathematics.

Xiaopeng Zhao, Major Professor

We have read this thesis and recommend its acceptance:

Suzanne Lenhart, Charles Collins

Accepted for the Council:
Carolyn R. Hodges

Vice Provost and Dean of the Graduate School

(Original signatures are on file with official student records.)

Border-Collision Bifurcations of Cardiac Calcium Cycling

A Thesis Presented for the

Master of Science

Degree

The University of Tennessee, Knoxville

Jacob Michael Kahle

December 2015

ACKNOWLEDGEMENTS

I would like to express my deep gratitude to Dr. Xiaopeng Zhao for his support and guidance during my time in graduate school. Special thanks also go to Dr. Zhao for providing me the opportunity to work with him studying cardiac dynamics, and for serving as my advisor. I would like to thank Dr. Suzanne Lenhart and Dr. Charles Collins for serving on my thesis committee as well. I would like to thank the Student Success Center at The University of Tennessee for providing me the great opportunity to work closely with undergraduate students throughout my time there, and for the much needed support through the ebbs and flows of graduate school.

Thanks also to my parents and siblings, for being understanding of my struggles and availability over the last three years, and to my beloved wife, for her continual and comprehensive support during our studies, both together and apart.

ABSTRACT

In this thesis, we study the nonlinear dynamics of calcium cycling within a cardiac cell. We develop piecewise smooth mapping models to describe intracellular calcium cycling in cardiac myocytes. Then, border-collision bifurcations that arise in these piecewise maps are investigated. These studies are carried out using both one-dimensional and two-dimensional mapping models. Studies in this work lead to interesting insights on the stability of cardiac dynamics, suggesting possible mechanisms for cardiac alternans. Alternans is the precursor of sudden cardiac arrest, a leading cause of death in the United States.

TABLE OF CONTENTS

LIST OF FIGURES

CHAPTER I

INTRODUCTION AND GENERAL INFORMATION

Every year, approximately 610,000 people die of heart disease in the United States—one out of every four deaths nationwide. On top of this staggering statistic, nearly 735,000 Americans have a heart attack each year [1]. These numbers are too large to ignore, providing insight into the fact that the heart is one of the most studied organs of the human body. The human heart is a four-chambered pump, consisting of two pumps arranged in series. Cardiac tissue is composed of cardiac muscle cells, which are both contractile and excitable. The excitability of these cardiac cells enables action potentials in a heart to propagate; however, the action potential causes cells to contract, which enables the pumping of blood throughout the body [2]. Cardiac action potentials begin in the sinoatrial (SA) node, and propagate as an electrical signal through the atria, atrioventricular (AV) node, and then into and throughout the ventricles. Heart disease causes wavebreaks, inducing potentially life-threatening reentrant arrhythmias [3].

John Cain [4] proposed six ongoing challenge problems that seem tractable, and which draw from a variety of mathematical subdisciplines. Most of these challenges involve cardiac electrophysiology studying electrical wave propagation in heart tissue. In 1952, Hodgkin and Huxley introduced a model of electrical propagation in the squid giant axon [5]. This model was deemed to be ahead of its time, and is the basis for most models proposed today. One such challenge proposed in Cain's work is called the "Modeling Challenge", wherein we try to keep the model minimally complicated so that it is amenable to mathematical analysis, but is sufficiently detailed so that it can

reproduce as much clinically relevant data as possible [4]. Another challenge proposed in Cain is referred to as the "Alternans Challenge", which is to derive a mathematical criterion that accurately predicts the onset of alternans [4]. Investigating cardiac alternans may lead to a better understanding of the mechanisms of cardiac arrhythmias. In time, we can expect that this will result in the implementation of better algorithms for the prediction and prevention of diseases caused by and related to these arrhythmias [6]. These challenges are the driving pieces behind this thesis.

Recent studies have demonstrated that the dynamic properties of cardiac excitation-contraction coupling play significant roles in identifying heterogeneities which promote arrhythmogenesis [7-8]. The cause for these dynamics is related to action potential properties, including action potential duration (APD) restitution, intracellular calcium cycling dynamics, and wave conduction properties [3].

When the pacing rate is slow, each individual stimulation gives rise to a single action potential (1:1 pattern); however, when the pacing rate becomes sufficiently fast, the 1:1 pattern might be replaced by a 2:2 pattern, which is known as electrical alternans [9-10]. This is observed when the APD alternates between short and long values. Due to the role that experiments have placed on alternans in developing ventricular arrhythmias, the Alternans Challenge proposed by Cain [4] is a crucial step in the detection and prevention of fatal arrhythmias [6]. These experiments have suggested that the elimination of cardiac alternans might prevent conduction block, thus preventing the occurrence of fibrillation [11-13]. Therefore, the overarching goal of this area of research is to understand the mechanism of alternans formation, which plays a vital role in the detection and prevention of fatal arrhythmias. It is well understood that alternans

develops under decremented pacing periods in cardiac tissue [6]. We couple this with the fact that the occurrence of ventricular arrhythmias has been linked to single-cell dynamics [14-15] to conclude that modeling the dynamics of a single cardiac cell under decrementing pacing periods will help us discover information regarding the onset of alternans.

At the cellular level, cardiac dynamics involves a bidirectional coupling between membrane voltage dynamics and intracellular calcium cycling [6]. Major interactions between action potential and Ca cycling in cardiac myocytes are illustrated in Figure 1 below [16]. This illustration demonstrates a process called calcium-induced calcium release (CICR). During CICR, calcium promotes its own release from intracellular calcium stores—in the case of a cardiac cell, the sarcoplasmic reticulum (SR) [17]. The depolarization of the T-tubule by action potential causes opening of the L-type Ca channel, and thus Ca flows into the cell. The Ca that entered the cell stimulates a release of additional Ca from the SR via ryanodine receptors (RyR). The released Ca diffuses through the myoplasm and binds to myofilaments, causing contraction, before being eventually removed from the myoplasm by adenosine triphosphatases (ATPases), which pump the cytoplasmic Ca either back into the SR or out of the cell entirely [2]. Membrane voltage dynamics has been extensively investigated in the literature. Throughout this thesis, we will instead study intracellular calcium cycling dynamics under voltage clamp conditions.

There are several modeling approaches that have been proposed in describing the dynamic behaviors of the heart, including ionic models, simplified models, and mapping models [18]. Our choice for describing the dynamics of the heart is via mapping models.

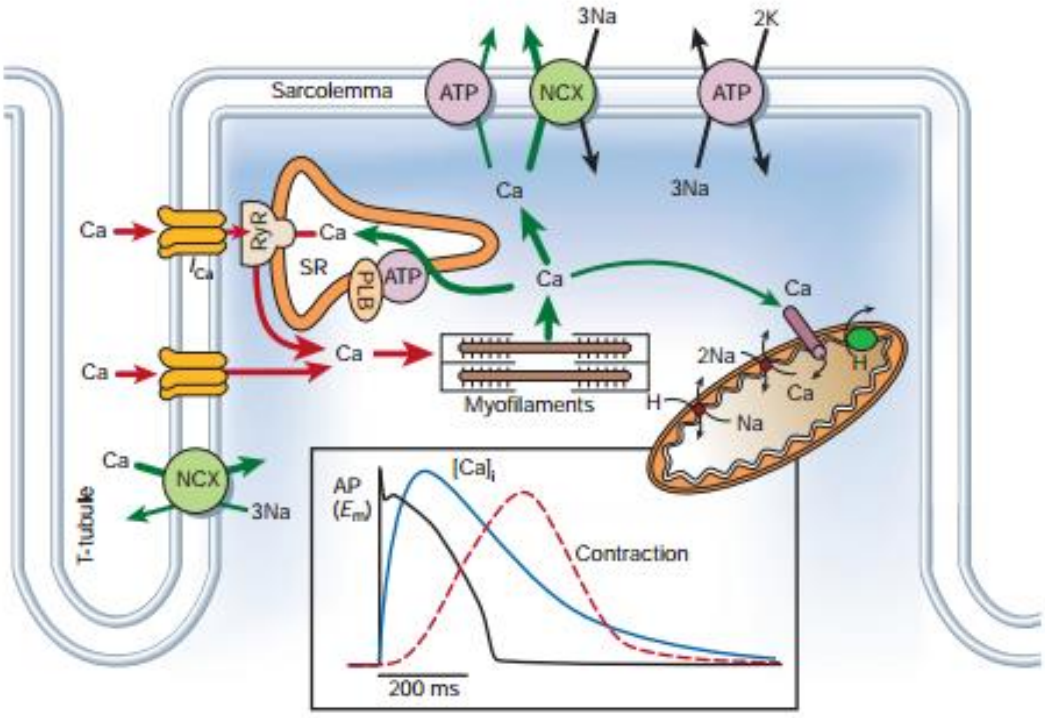

Figure 1 Ca transport in ventricular myocytes. Inset shows the time course of an action potential, Ca transient and contraction measured in a rabbit ventricular myocyte at 37°C; copied from Bers et al. [16].

First, we will develop a one-dimensional mapping model of intracellular calcium cycling and carry out a detailed bifurcation analysis of this model. Most experimental and theoretical studies assume that alternans in homogeneous cardiac tissue is determined only by the pacing period [6]. However, in order to reproduce experimentally obtained restitution data, the one-dimensional mapping should be replaced by a higher dimensional mapping [19]. This leads us to implement a two-dimensional mapping model, in which we utilize the intracellular calcium cycling and the diastolic interval to calculate action potential duration, which is presented in the second chapter.

CHAPTER II

LITERATURE REVIEW

First, we observe the current literature regarding calcium cycling in a cardiac cell, concentrating on a paper written in 2007 by Qu et al. [3]. This article developed iterated mapping models to study the nonlinear dynamics of cardiac excitation-contraction coupling. Previous studies, which have modeled CICR, have assumed that APD is a function of the preceding diastolic interval (DI). From Figure 1, we can see that Ca also has an effect on APD. Therefore, it is justifiable to assume that APD is a function of both the preceding DI, as well as the peak cytoplasmic Ca of the current beat. Hence, we use an equation of the form:

$$a_{n+1} = f\left(d_n, c_{n+1}^{p}\right), \tag{2.1}$$

where a_{n+1} is the APD of the $(n+1)$st beat, c_{n+1}^{p} is the peak cytoplasmic calcium of the $(n+1)$st beat, and d_n is the DI of the nth beat, and is taken to be:

$$d_n = T - a_n, \tag{2.2}$$

where T is the pacing period.

The relationship between APD and the previous DI is well-estimated from several experiments [20-21], and is known as the APD restitution function. The effect of Ca on APD, on the other hand, is a bit more irregular in that increased Ca can either shorten or lengthen APD, depending on the experimental conditions. To simplify the model, we separate Equation (2.1) into voltage dependent and Ca-dependent components, so that:

$$a_{n+1} = f(d_n) + p\left(c_{n+1}^{p}\right)a_{n+1}. \tag{2.3}$$

Currently, there is no experimental data to show the effect of Ca on APD, and so it was assumed in Qu et al. [3] that the magnitude of its effect is proportional to the APD of the same beat. Therefore, they defined $p(c_{n+1}^p)$ proportional to the peak cytoplasmic Ca at each beat, so that:

$$p(c_{n+1}^p) = \gamma c_{n+1}^p, \tag{2.4}$$

where γ is a parameter describing the strength of the Ca-to-APD coupling. According to the text [3], $\gamma > 0$ corresponds to positive Ca-to-APD coupling, and $\gamma < 0$ corresponds to negative Ca-to-APD coupling. In positive Ca-to-APD coupling, a large Ca release promotes Ca efflux via the electrogenic Na-Ca exchange, which generates an inward current and prolongs the APD, whereas a negative Ca-to-APD coupling occurs when a large Ca release inactivates the L-type Ca current more rapidly, possibly shortening the APD.

From Figure 2, we see that peak cytoplasmic Ca is the sum of diastolic cytoplasmic Ca (c_n) and the total Ca released (r_{n+1}) from the SR during the $(n+1)$th beat. We calculate c_{n+1}^pusing:

$$c_{n+1}^p = c_n + r_{n+1}. \tag{2.5}$$

We find diastolic cytoplasmic Ca (c_n) by finding the difference between the total cellular Ca (b_n) at the end of the nth beat, and Ca load in the SR (l_n) in the nth beat as below:

$$c_n = b_n - l_n. \tag{2.6}$$

Equations for total cellular Ca, SR Ca load, and Ca released from the SR will be introduced shortly.

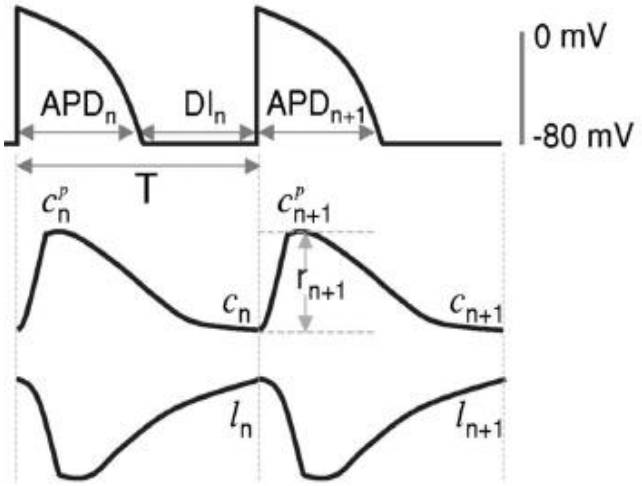

Figure 2 Graphical definitions of APD, DI, pacing period, T, diastolic Ca (c_n) at the end of each beat, peak cytoplasmic Ca (c_n^p), Ca released from SR (r_n), and SR load (l_n) at the end of each beat; copied from Qu et al. [3].

As aforementioned, the APD restitution function has been widely studied and compared with experimental results; thus, the APD restitution function will be given by

$$f(d_n) = A_0\left[1 - \frac{1}{1+e^{\frac{(d_n - D_0)}{\tau_0}}}\right] + A_1 e^{\frac{-(d_n - D_1)^2}{\tau_1}}, \tag{2.7}$$

where A_0, D_0, τ_0, A_1, D_1, and τ_1 are parameters. We will show the specific values to fit the APD restitution function in Figure 3. We can update the SR Ca load at each beat using the following equation:

$$l_{n+1} = l_n - r_{n+1} - z_{n+1} + u_{n+1}. \tag{2.8}$$

Here, we take the SR Ca load (l_n) at the end of the nth beat, subtract the Ca released (r_{n+1}) and the Ca leaked (z_{n+1}) from the SR during the $(n+1)$st beat, and finally add the Ca uptake (u_{n+1}) during the $(n+1)$st beat.

As evidenced experimentally, Ca released from the SR depends on SR Ca load and magnitude of L-type Ca current, which triggers Ca release from the SR during CICR [22]. However, the magnitude of the L-type Ca current during an action potential is dependent on the time of recovery from inactivation; thus, the amount of Ca released from the SR is directly related to the previous DI [23]. Therefore, in order to represent the dependence on SR Ca load and DI mathematically, we need to define the Ca released from the SR as:

$$r_{n+1} = q(d_n)g(l_n). \tag{2.9}$$

Here, $q(d_n)$ represents the restitution properties of SR Ca release. From experimental data, Qu et al. [3] defined this function to be:

$$q(d_n) = 1 - \sigma e^{-\frac{d_n}{\tau_q}}. \tag{2.10}$$

The function $g(l_n)$ from above represents the dependence of the SR Ca release on the SR Ca load. Again, from experimental measurements, the following equation was used:

$$g(l_n) = l_n\left[1 - \frac{1-\alpha}{1+e^{\frac{l_n - l_c}{\beta}}}\right]. \tag{2.11}$$

This function has been shown to fit experimental data by varying α, β, and l_c [3].

SR Ca leak is determined by SR Ca load, and so is included with the release function defined above, so that $g(l_n)$ represents both SR Ca leak and SR Ca release, based on SR Ca load. Uptake of Ca into the SR occurs via sarcoplasmic-endoplasmic reticulum Ca ATPase (SERCA) pumps (Figure 1) [16]. These pumps depend on basic cycle length, T, as well as the peak cytoplasmic Ca in the cell for a given beat. Hence:

$$u_{n+1} = u(T)h(c^p_{n+1}). \tag{2.12}$$

In Equation (2.12), $u(T)$ shows the dependence on time duration of pumping, and is modeled using:

$$(2.13) \qquad u(T) = 1 - \rho e^{-\frac{T}{\tau_u}},$$

Now notice that $h\left(c_{n+1}^{p}\right)$ above is the SR Ca uptake function depending on peak cytoplasmic Ca. Qu et al. [3] assume this uptake function to be defined via:

$$(2.14) \qquad h\left(c_{n+1}^{p}\right) = \nu c_{n+1}^{p}\left[1 - \frac{1}{1+e^{\frac{c_{n+1}^{p} - c_0}{\theta}}}\right],$$

Finally, we choose to update the total cellular Ca by using the following function:

$$(2.15) \qquad b_{n+1} = b_n - \kappa[c_n - c(T)] + \eta(a_{n+1} - a_n),$$

where $c(T)$ represents steady state cytoplasmic Ca at a given cycle length T, κ is a constant, and η depends on positive/negative APD-to-Ca coupling, as γ did inversely. Notice then, at equilibrium, $a_{n+1} = a_n$, and so the APD would have no effect on updating the total cellular Ca at each beat; however, at periodic or chaotic states, the amount of Ca can vary drastically from beat-to-beat. Lastly, they [3] defined the steady state cytoplasmic at a given cycle length T using:

$$(2.16) \qquad c(T) = c_1(1 + \varepsilon e^{-\frac{T}{\tau_c}}),$$

where ε and τ_c are constants.

Utilizing the equations established here to model the physiology of a cardiac cell, we can investigate several items. First, we can analyze stability of the model, which has been done by Qu et al. [3]. In this thesis, we simplify the model to study only the intracellular components to understand Ca cycling within the SR. We then proceed to study beat-to-beat Ca cycling, with period-dependent release and uptake. Finally, we

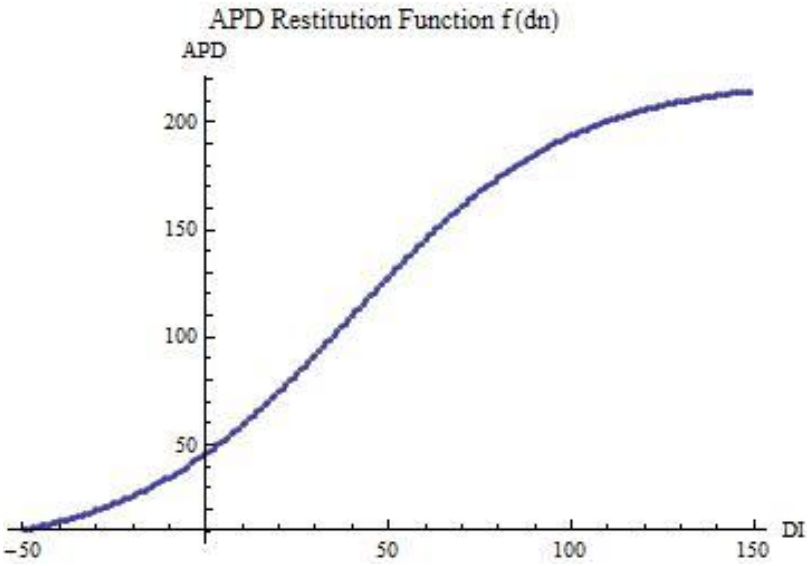

Figure 3 Diastolic interval plotted against APD, Equation (2.7). No dependence of peak cytoplasmic Ca on APD. Constants in $f(d_n)$ given by: $A_0 = 220$; $d_0 = 40$; $\tau_0 = 30$; $A_1 = 0$.

analyze APD and Ca cycling dynamics together, so that the APD at each beat depends on both DI as well as peak cytoplasmic Ca. An initial look at diastolic interval vs. action potential duration is shown in Figure 3. This plot does not include peak cytoplasmic Ca in updating the restitution function, but instead relies only on the previous DI.

There is, however, a process to follow in simulating these equations to understand cycling of Ca in the heart. Before we begin, we observe the variables and their representations in Table 1. This will allow us to keep track of what physiological process is being represented by each variable. Next, we define the selection of equations we are using in Mathematica. Obviously, for different simulations with different assumptions, these equations will have changing parameter values. These parameter values will be the influence on the dynamics of our system. Next, we define our initial conditions for our

Table 1 This table displays the variables used in Chapter 2, as well as each variable's physiological representation.

a_{n+1}	APD of (n+1)st beat
b_n	Total cellular calcium of the nth beat
c_{n+1}^{p}	Peak cytoplasmic calcium of the (n+1)st beat
c_n	Cytoplasmic calcium at the end of the nth beat
d_n	DI of nth beat
l_n	SR calcium load at the end of the nth beat
r_{n+1}	SR calcium release during the (n+1)st beat
T	Basic cycle length, or pacing period
u_{n+1}	SR calcium uptake during the (n+1)st beat
z_{n+1}	SR calcium leak during the (n+1)st beat

variables, which were always SR Ca load, total cellular Ca, and APD; these initial conditions are irrelevant because our mapping model will converge to the steady state regardless of initial conditions. All other variable values can be calculated using these initial conditions. We then cycled through our equations, again depending on our parameters and assumptions. In order to see convergence to the steady state, we simulated 250 beats at each pacing period, keeping all of the information from the last 100 beats. We calculated the steady state cytoplasmic Ca first, followed by the portion of the Ca uptake function dependent on pacing period. Then we calculated the length of the diastolic interval, and used that information to find the Ca released from the SR in the $(n+1)$st beat, in equations (2.10) and (2.11). Next, we found cytoplasmic Ca at the end of the nth beat, and proceeded to calculate the peak cytoplasmic Ca, the total cellular Ca, and the SR Ca load of the $(n+1)$st beat. Finally, we calculated the APD of the $(n+1)$st beat before cycling back through these equations in the same order. Again, for several of

the simulations implemented in this paper, we did not use each equation, in which case we would simply remove those steps of the process.

In the first simulation (results shown in Figure 4), we fixed the intracellular Ca level from beat to beat, and allowed for period-independent SR Ca release and uptake. Although there is no physiological evidence that this actually occurs in a cardiac cell [3], it is important to fully understand intracellular Ca cycling alone. The simplifications in this simulation result in a linear mapping model, where the restitution function is independent of the peak cytoplasmic Ca. Notice that here, since SR Ca release and uptake are period- independent, Equation (2.11) represents the SR Ca release, and Equation (2.14) represents SR Ca uptake, so that Equation (2.8) becomes:

$$l_{n+1} = l_n - g(l_n) + h\left(c_{n+1}^p\right). \tag{2.17}$$

Also, because total cellular Ca is fixed, Equation (2.6) becomes:

$$c_n = b - l_n. \tag{2.18}$$

This simulation gives the results shown in Figure 4. Parameters for $g(l_n)$ and $h\left(c_{n+1}^p\right)$ are given in the captions for Figure 4.

Now, we make the model more complex. In the previous simulation, we assumed the total cellular Ca to be constant, whereas now we assume the total cellular Ca is changing from beat to beat. Also, to make this simulation even more comparable to human physiology, we account for period-dependent SR Ca release and SR Ca uptake. This has been experimented under voltage clamp conditions, which was used as a basis for the development of this model [3]. Finally, because we are updating SR Ca release and uptake based on the pacing period, we analyze APD along with Ca cycling dynamics

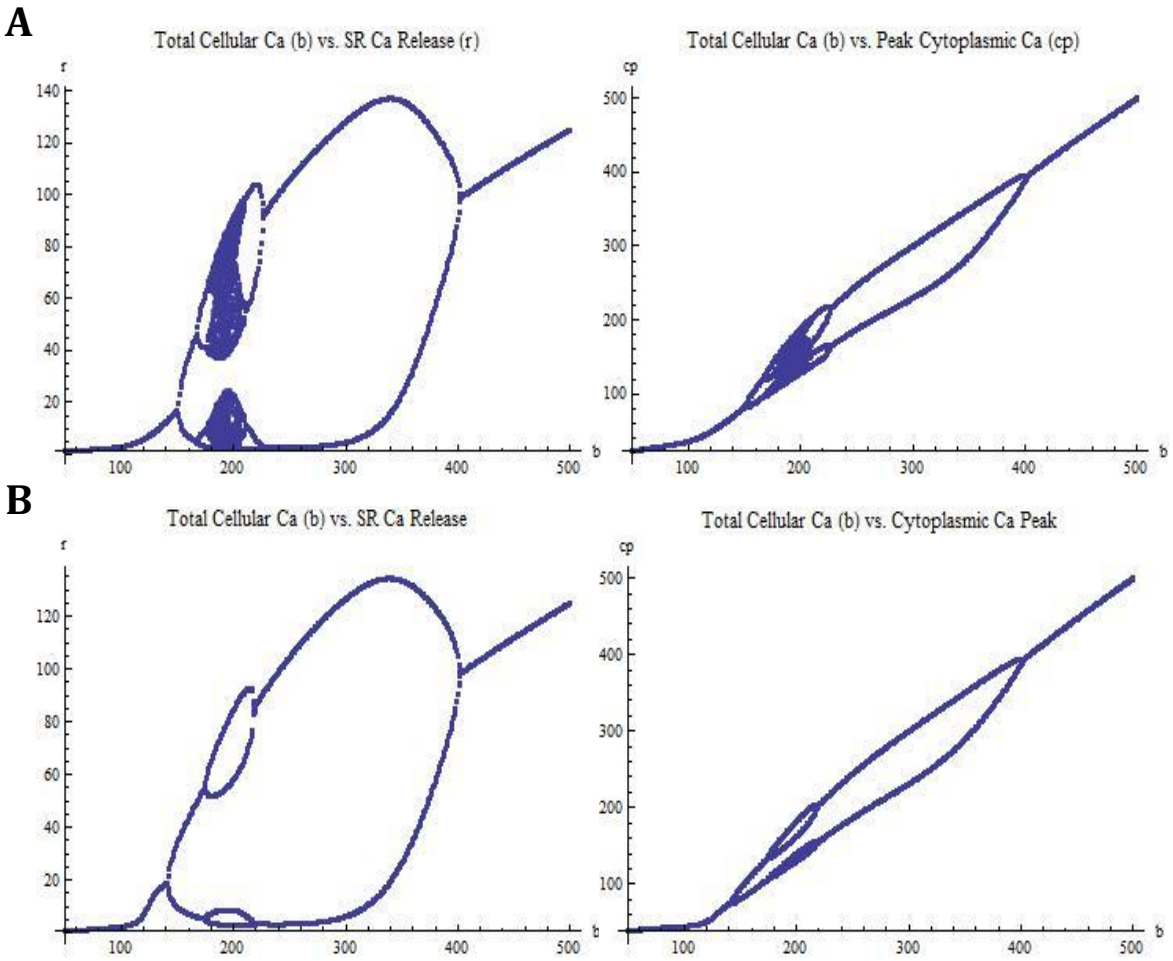

Figure 4 Dynamics due to nonlinear, period-independent SR Ca release and uptake when total cellular Ca is constant. Total cellular Ca compared with SR Ca release and peak cytoplasmic Ca, given the following values for $g(l_n)$ and $h\left(c_{n+_1}^{p}\right)$: (A) $\alpha = 0.036;\ l_c = 93.5;\ \beta = 5;\ \nu = 0.25;\ c_0 = 50; \theta = 20$. (B) $\alpha = 0.036;\ l_c = 93.5;\ \beta = 6;\ \nu = 0.25;\ c_0 = 50; \theta = 4$.

during this simulation. This is the most realistic simulation that can be accomplished using this model because we are updating each represented physiological aspect of the cardiac cell from beat to beat, including each beat's APD, DI, total cellular Ca, SR Ca load, peak cytoplasmic Ca, etc. Here, we are updating the APD of each beat based on the previous DI, along with the peak cytoplasmic Ca. Thus, during this simulation, we are using each mathematical equation defined previously. Results are posted in Figure 5.

One interesting feature of these plots is the interval of quasiperiodicity in each. This occurs from $T = 220$ until $T = 235$ in each of the plots above, and leads to some interesting results in itself. Thus, we know that, by fixing T, we can plot any other two values and achieve a seemingly periodic result, for example APD vs. SR Ca released and APD vs. total cellular Ca, which are posted in Figure 6.

At the beginning of the chapter, we plotted the restitution function $f(d_n)$, and did not utilize Ca to calculate APD. Now, however, we include Ca in updating APD, thus calculating APD utilizing Equation (2.3). We were able to plot DI vs. APD, as before, using the same parameters in $f(d_n)$ as in Figure 3. Our results were quite interesting, comparing extremely well to the Ca-independent system, and can be seen in Figure 7.

One extremely fascinating output from these simulations is total cellular Ca vs. SR Ca released. This is one of the focal points of Figure 4, before pacing periods and APD were taken into account, as will be shown in Figure 8; also recall that for our results in Figure 4, we were assuming fixed intracellular Ca levels from beat to beat. We now take another look at the correlation between total cellular Ca and SR Ca released in Figure 8, hoping to gain some insight into this curious relationship. The results in Figure 8 demonstrate the importance of APD and pacing period, T, on Ca cycling within the cell.

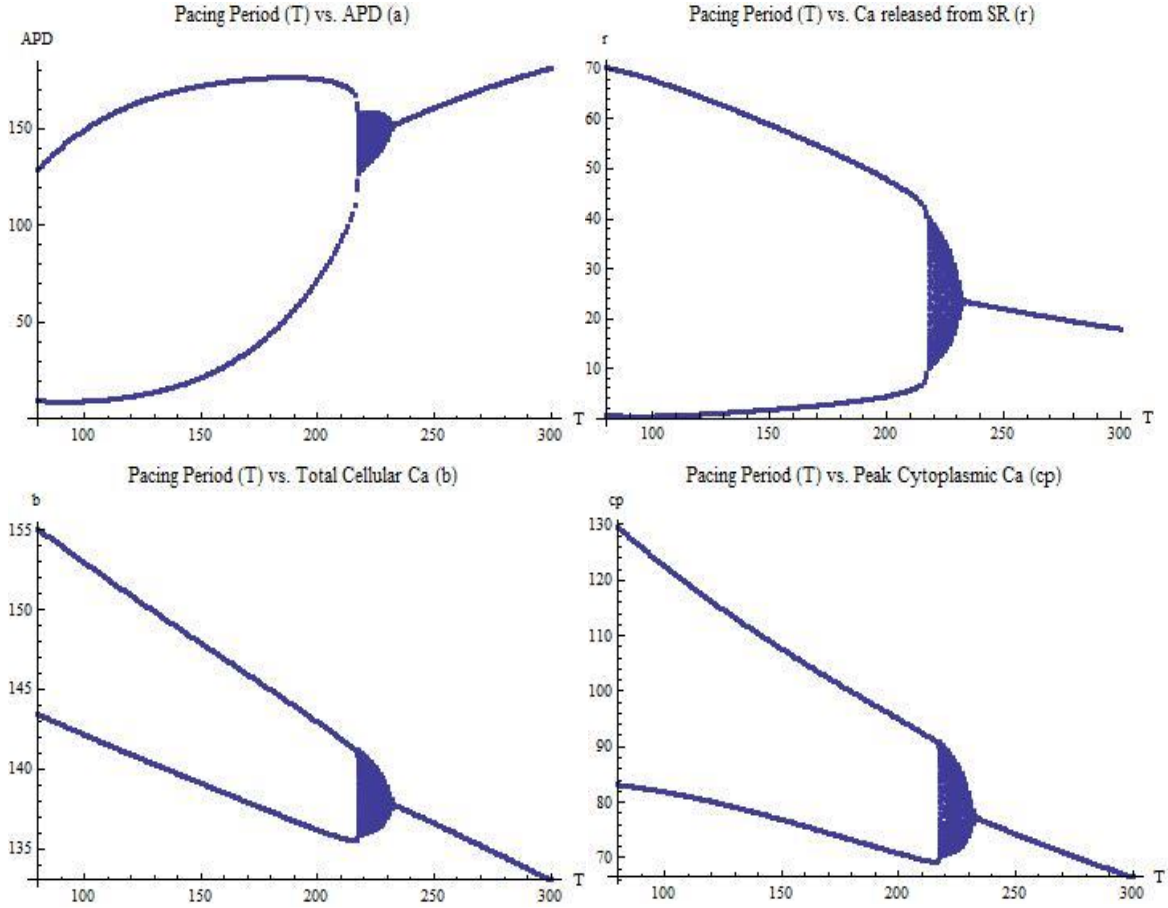

Figure 5 Dynamics due to nonlinear, period-dependent SR Ca release and uptake, varying total cellular Ca. Pacing period compared with APD, SR Ca release, total cellular Ca, and peak cytoplasmic Ca, given these values for parameters in the above equation: $\alpha = 0.036;\ l_c = 93.5;\ \beta = 5;\ \nu = 0.4;\ c_0 = 50; \theta = 20; \kappa = 0.2; \gamma = -0.002;\ A_0 = 220;\ d_0 = 40;\ \tau_0 = 30; \eta = 0; \sigma = 0.5;\ \tau_q = 80; \rho = 0.15;\ \tau_u = 200; c_0 = 20;\ \varepsilon = 2;\ \tau_c = 300.$

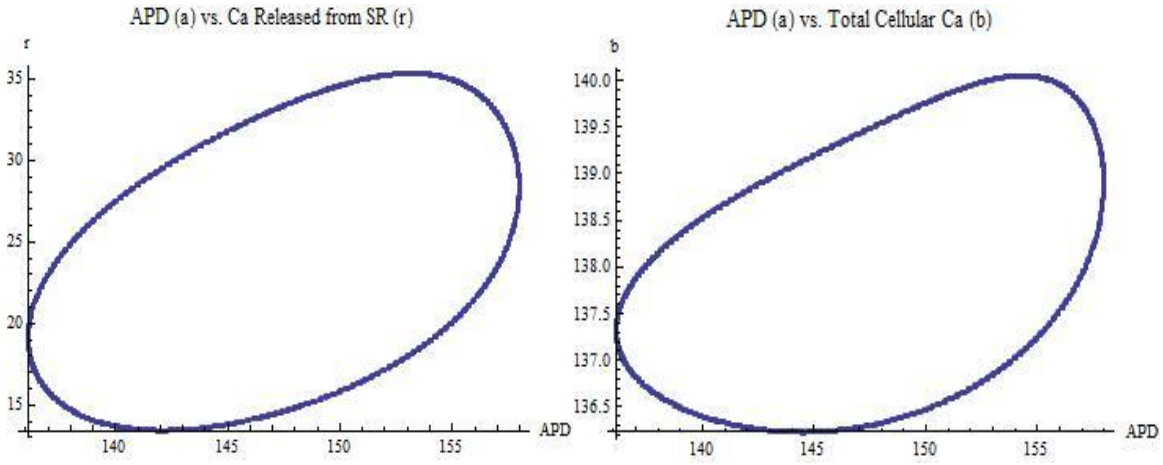

Figure 6 Quasiperiodicity dynamics due to nonlinear, period-dependent SR Ca release and uptake, varying total cellular Ca. APD compared with SR Ca release and total cellular Ca, given the same values for parameters as in Figure 5. Here, we set $T = 225$. Instead of iterating through 250 beats and keeping information from the last 100, we iterated through 2500 beats and kept information from the last 2150.

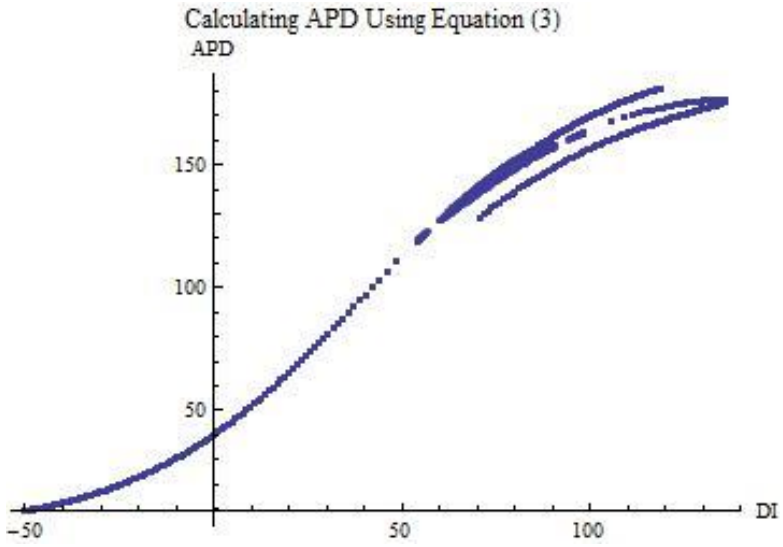

Figure 7 Diastolic interval plotted against APD, Equation (2.3). Includes dependence of peak cytoplasmic Ca on APD. Constants given in Figure 5.

Note that our parameters are essentially identical between Figure 4 and Figure 8, except that in the latter we are simulating other physiological aspects of the cardiac cell.

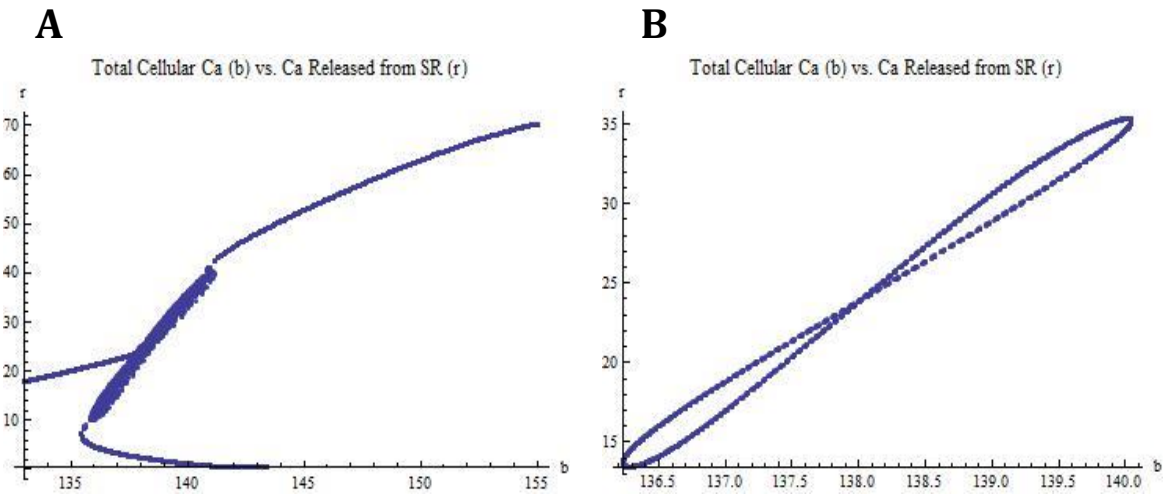

Figure 8 Dynamics due to nonlinear, period-dependent SR Ca release and uptake, varying total cellular Ca. Total cellular Ca compared with SR Ca release, given the same values for parameters as in Figures 5 and 6. (A) This simulation was run from $T = 80$ to $T = 300$, as in Figure 5. We record each beat's total cellular Ca as well as SR Ca released, simulating 250 beats for each pacing period. (B) Here, we construct similarly to Figure 6, iterating 2500 beats and keeping the information from the last 2350. Again, we set $T = 225$.

CHAPTER III

ONE-DIMENSIONAL MAPPING MODEL

Motivated by the theoretical study in Yorke et al. [24], we propose a piecewise return map to describe intracellular calcium cycling. We consider a piecewise return map on the peak calcium transients at beat n, which has been represented as c_n^p. We define the return map to be:

$$c_{n+1}^p = \begin{cases} g1[c_n^p] & c_n^p > C0 \\ g2[c_n^p] & c_n^p < C0' \end{cases} \tag{3.1}$$

where

$$\begin{aligned} g1[Ca] &= \mu * B + s1 * (Ca - C0) + C1 \\ g2[Ca] &= \mu * B + s2 * (Ca - C0) + C1. \end{aligned} \tag{3.2}$$

For simplicity in this model, we let Ca represent peak calcium transients in the cytoplasm, and we let B represent basic cycle length. There exists a threshold, $C0$, such that when $Ca > C0$, the calcium recovery takes a shallow slope, $s1$, whereas it takes a steeper slope, $s2$, when $Ca < C0$. The map, however, is continuous at $C0$, with a discontinuous, linear derivative. In studying the fixed points of our return map, we see that he fixed point at $C0$ satisfies

$$C0 = \mu * B + s1 * (C0 - C0) + C1,$$

so that

$$C0 - C1 = \mu * B.$$

We let $C0 = 1.5\ \mu M$, and we let $C1 = 0.5\ \mu M$. We suppose bifurcation occurs at 200 ms, which then provides us with $\mu = 5 * 10^{-3}\ \mu M/ms$. According to Yorke et al.

[24], the map may exhibit different behaviors depending on the values of the two slopes, $s1$ and $s2$. We set $-1 < s1 < 1$ to ensure stable periodic response under long pacing periods. We then examine the response for different values of $s2$. If $s2 < -1 < s1 < 0$ and $s1 * s2 < 1$, then a border-collision period-doubling bifurcation occurs. When $s2 < -1 < s1 < 0$ and $s1 * s2 > 1$, a period-1 response leads to no attractor. Finally, if $0 < s1 < 1$ and $s2 < -1$, a period-1 solution bifurcates to either a periodic attractor or a chaotic attractor [3,24]. We pay particular attention to the case $0 < s1 < 1$ and $s2 < -1$.

We define the return map as follows:

$$g[Ca] \coloneqq \begin{cases} \mu * B + s1 * (Ca - C0) + C1 & Ca > C0 \\ \mu * B + s2 * (Ca - C0) + C1 & Ca \leq C0 \end{cases}. \tag{3.3}$$

Notice that, since we are interested in the dynamics that result with varying $s1$ and $s2$ values, we can set $C0 = 0$, so that we can observe a bifurcation at $Ca = 0$, rather than at $Ca = 1.5$; after all, the dynamics will not be affected by a translation of the plot. We take a look at the modified system of equations:

$$g[Ca] \coloneqq \begin{cases} \mu * B + s1 * Ca + C1 & Ca > 0 \\ \mu * B + s2 * Ca + C1 & Ca \leq 0 \end{cases}. \tag{3.4}$$

From Yorke et al. [24], where we are given the piecewise return map

$$f[x] \coloneqq \begin{cases} ax + \eta & x \leq 0 \\ bx + \eta & x > 0 \end{cases}, \tag{3.5}$$

we know that the map $f[x]$ is invariant under the transformations $x \to -x$, $\eta \to -\eta$, $a \leftrightarrow b$. Thus, any bifurcation that occurs as η increases (decreases) through zero also occurs as η decreases (increases) through zero if we interchange the values of a and b. From this, we know that our map given in Equation (3.4) is invariant under the transformations $Ca \to -Ca$, $\mu * B + C1 \to -(\mu * B + C1)$, $s1 \leftrightarrow s2$. Using these facts,

we can alter the function once again to obtain a left-to-right border-collision bifurcation given by:

$$g[Ca] \coloneqq \begin{cases} \mu * B + s1 * Ca + C1 & Ca \leq 0 \\ \mu * B + s2 * Ca + C1 & Ca > 0 \end{cases}. \tag{3.6}$$

We can now apply the results from Yorke et al. [24] to the above Equation (3.6) to learn about the dynamics of the piecewise Equation (3.4) above. In the paper written by Yorke et al. [24], we have the piecewise equation given by Equation (3.5) here. In order to apply those results to our Equation (3.6) above, we define:

$$\begin{gathered} x = Ca; \\ a = s1; \\ b = s2; \\ \eta = \mu * B + C1; \\ f[x] = g[Ca]. \end{gathered} \tag{3.7}$$

Thus, we have the family of skew tent maps for which the results are discussed in Yorke et al. [24]. Therefore, we are interested in the $s1$-$s2$ region where $0 < s1 < 1$ and $s2 < -1$. Also, then, we have a bifurcation present itself at $0 = \mu * B + C1$ in our Equation (3.6), so that $-C1 = \mu * B$. Because we need to translate our function in order to obtain the original function, given by Equation (3.3), we will have a bifurcation at $C0 = \mu * B + C1$, so that $C0 - C1 = \mu * B$, as stated previously. We then have the following results.

We know that we will obtain a period-1 response leading to a period-m attractor $(2 \leq m \leq 7)$ when $0 < s1 < 1$ and $s2 < -1$ lie within specific regions which, according to Yorke et al. [24], are given by:

$$P_m = \left\{(s1, s2) \epsilon R : \; -s1^{1-m} < s2 < \frac{s1}{1 - s1}(1 - s1^{1-m})\right\}.$$

We see these regions given in Figure 9 below. The values of $s1$ and $s2$ which satisfy $0 < s1 < 1$ and $s2 < -1$ and lie outside of every P_m for $2 \leq m \leq 7$ result in a period-1 attractor leading to a chaotic attractor. As discovered in this study, as well as others [25-26], we can also find interesting results in this chaotic region (shown in grey in Figure 9), which will be discussed in further detail later.

First, we study period-1 to period-m responses, starting with a period-2 attractor. We know that, if $0 < s1 < 1$ and $s2 < -1$ are such that $(s1, s2) \epsilon P_m$, then $(s1, s2)$ produce a period-m attractor; thus, in order to obtain a period-2 attractor, we need to satisfy:

$$-s1^{1-2} < s2 < \frac{s1}{1 - s1}(1 - s1^{1-2}).$$

Hence, we must satisfy the inequality:

$$-s1^{-1} < s2 < \frac{s1}{1 - s1}(1 - s1^{-1}),$$

and so,

$$-\frac{1}{s1} < s2 < -1.$$

Therefore, we expect a period-2 response when $0 < s1 < 1$ and $-1 < s1s2$. Now if we fix $s1$, we should be able to find $s2$ values satisfying these inequalities. For now, we set $s1 = 0.3$. Then $s2 > -\frac{1}{0.3}$, so that $s2 > -\frac{10}{3}$. Thus, when $s1 = 0.3$ and $s2 = -2 > -\frac{10}{3}$, we will observe a period-2 response, as shown in Figure 10A. Therefore, our results present exactly as we would expect, given the regions in Figure 9.

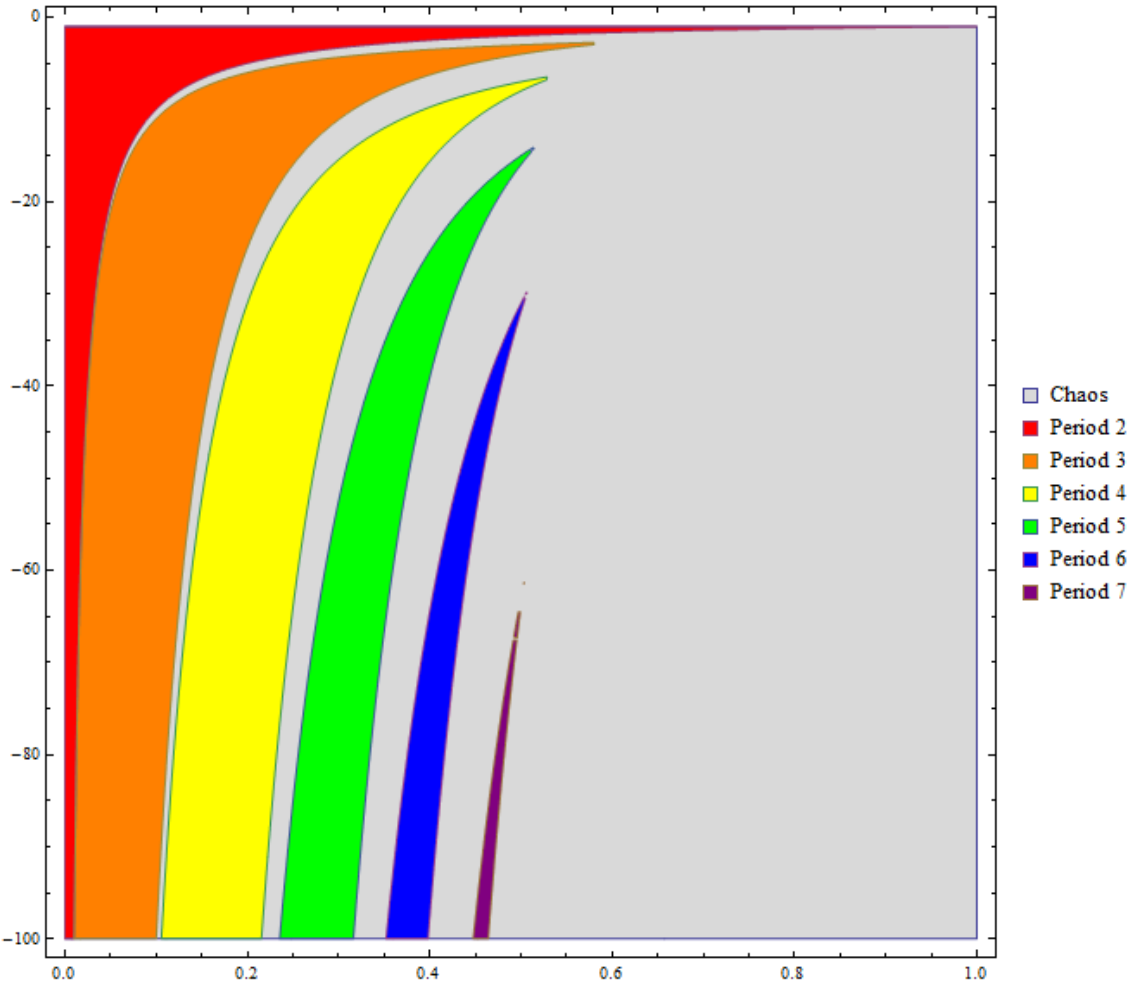

Figure 9 This figure shows regions in the $(s1, s2)$-space. If $(s1, s2)$ is in the grey region, then Equation (3.3) has a chaotic attractor; however, when $(s1, s2)$ lies within one of the other labeled regions, we know that Equation (3.3) has an attracting period-m orbit; recreated from Yorke et al. [24].

We check more regions. We aim to obtain a period-3 response. By setting $s1 = 0.2$, we know

$$-s1^{1-3} < s2 < \frac{s1}{1-s1}(1-s1^{1-3})$$

$$\Rightarrow -0.2^{-2} < s2 < \frac{0.2}{1-0.2}(1-0.2^{-2})$$

$$\Rightarrow -25 < s2 < -6.$$

Hence, if we choose any $s2$ satisfying the above inequalities, we should obtain a period-3 response. We choose $s2 = -6.75$, and our results are shown in Figure 10B. Following this same pattern, we were able to test period-1 solutions bifurcating to a period-m attractor, for $m = 2, \dots, 7$. Results are posted in Figure 10 with $(s1, s2) \epsilon P_m$, for $m = 2, \dots, 5$.

Let us now discuss some scenarios in which Equation (3.3) has a chaotic attractor. For every integer $m \geq 2$, let us assume that $(s1, s2) \epsilon (0,1) \times (-\infty, -1)$ is a chaotic pair, so that Equation (3.3) will indeed have a chaotic attractor. We assume also that $(s1, s2) \epsilon C_m(s1)$, where $C_m(s1)$ represents the component of the intersection of the vertical line through $(s1, s2)$ and the chaotic region that contains $(s1, s2)$, and the end points of $C_m(s1)$ are in ∂P_m and ∂P_{m+1} and are exactly $(s1, -s1^{1-m})$ and $\left(s1, \frac{s1}{1-s1}(1 - s1^{-m})\right)$. Then there exist intervals for $s2$ in $C_m(s1)$, depending on $s1$, such that one of the following must hold:

(i) $2^k m$-piece chaotic attractor (for some $k \geq 1$);

(ii) m-piece chaotic attractor;

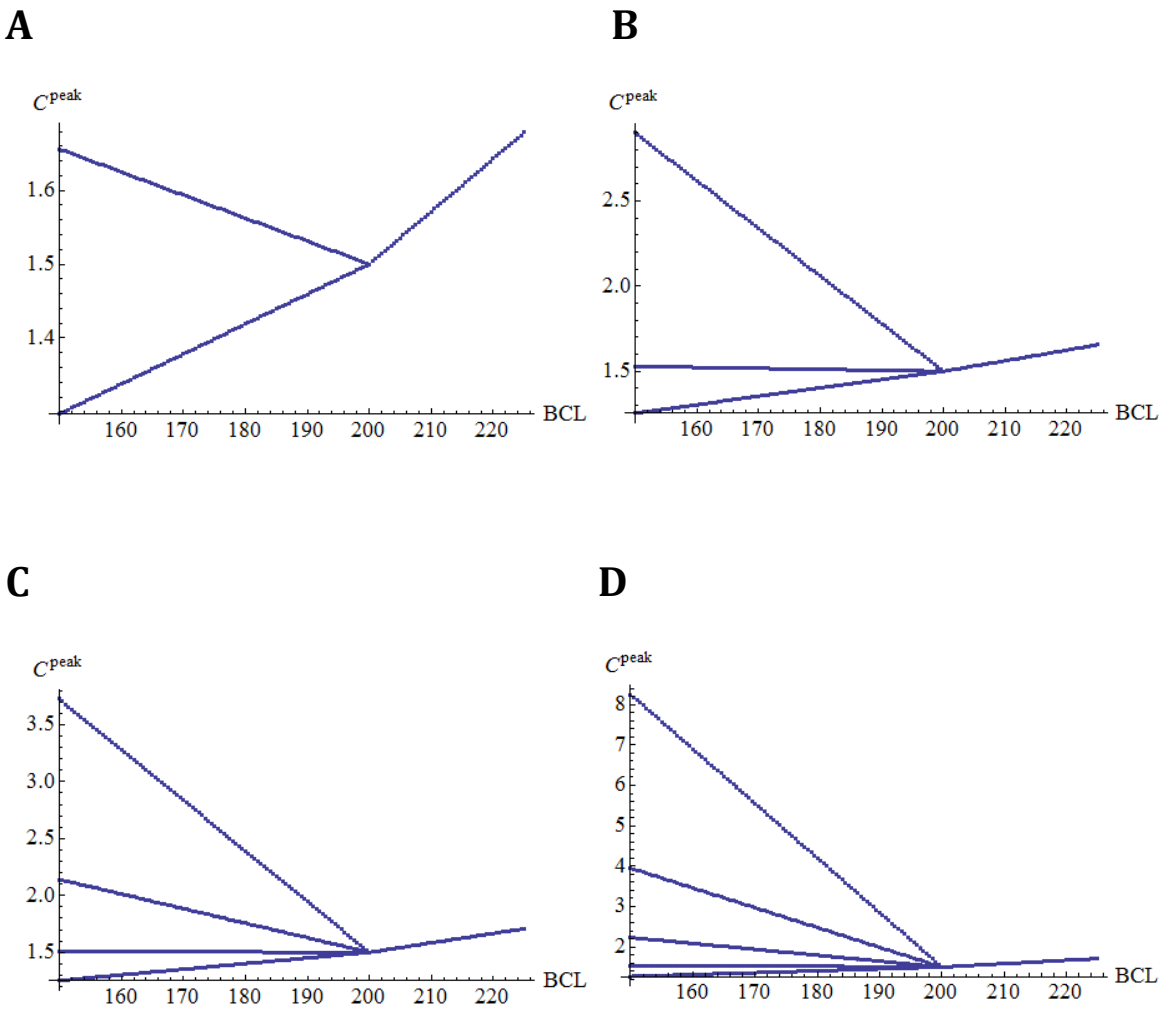

Figure 10 This figure shows a period-1 attractor leading to a period-m response: (A) period-1 → period-2; $s1 = 0.3$, $s2 = -2$; (B) period-1 → period-3; $s1 = 0.2$, $s2 = -6.75$; (C) period-1 → period-4; $s1 = 0.4$, $s2 = -10$; (D) period-1 → period-5; $s1 = 0.4$, $s2 = -30$.

(iii) one-piece chaotic attractor.

Details of each of these cases, including in what intervals such results will occur in $C_m(s1)$ for a given $s1$ and m, as well as dependencies on $s1$ in determining such intervals, have been provided previously and studied extensively by several researchers [24-26].

Our first tested case will demonstrate a one-piece chaotic attractor. We choose $s1 = 0.4$. In this case, we decide to examine a region inside of $C_3(0.4)$. We know that we must satisfy

$$\frac{0.4}{1-0.4}(1-0.4^{-3}) < s2 < -0.4^{1-3},$$

and so

$$-9.75 < s2 < -6.25$$

must be satisfied. Therefore, we choose $s2 = -9.5$, and obtain the result shown in Figure 11A, a one-piece chaotic attractor.

Next, we are working to find a $2^k m$-piece chaotic attractor. We set $s1 = 0.3$, and look into the region $C_2(0.3)$. Now, we know that $s2$ must satisfy the following inequalities in order to lie within this region:

$$\frac{0.3}{1-0.3}(1-0.3^{-2}) < s2 < -0.3^{1-2}.$$

Thus,

$$-\frac{13}{3} < s2 < -\frac{10}{3}.$$

We choose $s2 = -3.5$ in order to derive our desired $2^k m$-piece chaotic attractor, where $k = 1$ in this case. Thus, we should observe a 4-piece chaotic attractor (Figure 11B).

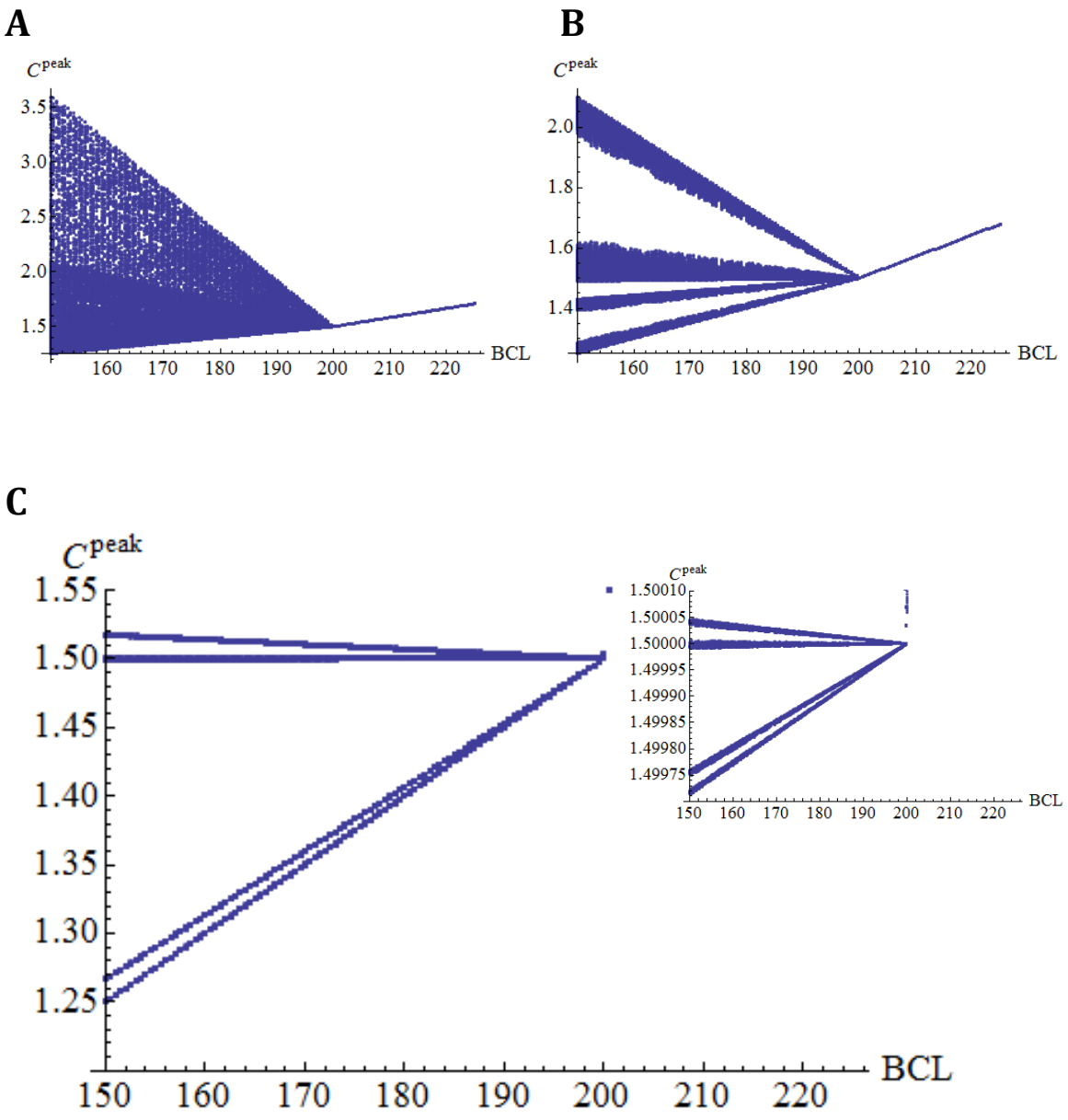

Figure 11 This figure shows a period-1 attractor leading to a chaotic response: (A) period-1 → 1-piece chaotic attractor; $s1 = 0.4$, $s2 = -9.5$; (B) period-1 → 4-piece chaotic attractor; $s1 = 0.3$, $s2 = -3.4$; (C) period-1 → 16-piece chaotic attractor; $s1 = 0.95$, $s2 = -1.07$. Inset plot highlights the second of the four chaotic regions in the larger plot, demonstrating that this is truly a 16-piece chaotic attractor.

Our final result from the one-dimensional border-collision bifurcation analysis comes from the article written by Yorke et al. [24]. In their research, they deduce that we can find a $2^k m$-piece chaotic attractor when $m = 2$ using their proposed theorems. At the conclusion of the study, they propose that $s1 = 0.95$ and $s2 = -1.09$ should provide a sixteen-piece chaotic attractor from Equation (3.3), so that $k = 3$. In Figure 11C, we confirm their theoretical analysis by providing a plot showing this sixteen-piece chaotic attractor using our mapping model.

While this one-dimensional approach certainly provides us with some interesting results, many of these results do not actually occur physiologically. This is likely due to an oversimplification in the model, driving us to create a more complex two-dimensional model to describe intracellular calcium cycling.

CHAPTER IV

TWO-DIMENSIONAL MAPPING MODEL

In this chapter, we develop a two-dimensional mapping model to examine calcium dynamics in a cardiac cell under voltage clamp conditions. First, we examine the equations from Qu et al. [3] presented previously in Chapter 2. Recall that:

$$l_{n+1} = l_n - r_{n+1} - z_{n+1} + u_{n+1}, \tag{4.1}$$

and

$$b_{n+1} = b_n - \kappa[c_n - c(T)] + \eta(a_{n+1} - a_n). \tag{4.2}$$

In our desired two-dimensional mapping model, we will assume constant action potential duration (APD) from beat to beat. Thus, $a_{n+1} - a_n = 0$, and so Equation (4.2) can be simplified to be

$$b_{n+1} = b_n - \kappa[c_n - c(T)]. \tag{4.3}$$

As discussed in Chapter 2, we will assume that calcium leak will be included in our calcium release function. Since SR Ca release and uptake are period-independent, Equation (2.11) represents the SR Ca release, and Equation (2.14) represents SR Ca uptake, so that Equation (4.1) becomes

$$l_{n+1} = l_n - g(l_n) + h\left(c_{n+1}^p\right), \tag{4.4}$$

as was written and discussed at length in Chapter 2. Combining Equations (4.3) and (4.4) leads to the two-dimensional return map given by

$$\begin{cases} l_{n+1} = l_n - g(l_n) + h\left(c_{n+1}^p\right) \\ b_{n+1} = b_n - \kappa[c_n - c(T)] \end{cases}, \tag{4.5}$$

where l_n represents the calcium load in the sarcoplasmic reticulum (SR) at the end of the nth beat, b_n represents the total cellular calcium at the end of the nth beat, c_{n+1}^p represents peak cellular calcium during the (n+1)st beat, and κ is a constant, which we will take to be 0.5. We define $c(T)$ by

$$(4.6) \qquad c(T) = 28\left(1 + 2e^{-\frac{T}{300}}\right),$$

as in Chapter 2. Similarly, we define our functions $g(l_n)$ and $h\left(c_{n+1}^p\right)$ as written in Equation (2.11) and Equation (2.14), respectively, from Chapter 2:

$$(4.7) \qquad g(l_n) = l_n\left[1 - \frac{1 - 0.036}{1 + e^{\frac{l_n - 93.5}{5}}}\right]$$

$$(4.8) \qquad h\left(c_{n+1}^p\right) = 0.4c_{n+1}^p\left[1 - \frac{1}{1 + e^{\frac{c_{n+1}^p - 50}{4}}}\right]$$

Before we begin discussing modifications made to this original model, we recall the table of variables that was presented in Chapter 2, as seen in Table 2. Observe the two-dimensional bifurcation diagram presented by the original system of equations.

Table 2 This table displays the variables used in Chapter 4, as well as each variable's physiological representation.

a_{n+1}	APD of (n+1)st beat
b_n	Total cellular calcium of the nth beat
c_{n+1}^p	Peak cytoplasmic calcium of the (n+1)st beat
c_n	Cytoplasmic calcium at the end of the nth beat
d_n	DI of nth beat
l_n	SR calcium load at the end of the nth beat
r_{n+1}	SR calcium release during the (n+1)st beat
T	Basic cycle length, or pacing period
u_{n+1}	SR calcium uptake during the (n+1)st beat
z_{n+1}	SR calcium leak during the (n+1)st beat

These diagrams are shown in Figure 12. In Figure 12A, we show the bifurcation diagram plotting b_n vs. l_n, and then include the varying parameter, T, in Figure 12B. This gives us an idea of where we begin with our study, and we will continue to compare our modified system to these original bifurcation diagrams throughout this section.

We aim to develop a piecewise linear approximation of the model. First, we create a piecewise linear approximation to our function $g(l_n)$, as shown in Figure 13. In determining the linear approximation for $g(l_n)$, we first notice that there are three nearly linear parts presented in this original function, with respect to l_n. Thus, we define a slope for the first third of the graph, as well as a slope for the last third of the graph. Then, we select a reference point, in this case $l_n = 95$. We find the slope at this point, and use that slope to determine the line tangent to $g(l_n)$ at $l_n = 95$, going on to calculate where that tangent line intercepts with our two previous lines; we call these intersections thresholds, th_1 and th_2. This gives rise to the function which will replace $g(l_n)$ in our model:

$$g_{lin}(l_n) = \begin{cases} \frac{3}{40} l_n & l_n < th_1 \\ 5.0673 l_n - 425.362 & th_1 \leq l_n < th_2 \\ l_n & th_2 \leq l_n \end{cases}.$$

This $g_{lin}(l_n)$ is the equation plotted in purple in Figure 13 above.

One observation made in substituting this $g_{lin}(l_n)$ equation into the analysis done in Chapter 2 of this text is that, while $T \geq 150$, l_n never rises above 90. Thus, we run simulations excluding the third linear part of $g_{lin}(l_n)$, and observe no difference in our results. Thusly, we instead define $g_{lin}(l_n)$ to be:

$$g_{lin}(l_n) = \begin{cases} \frac{3}{40} l_n & l_n < th_1 \\ 5.0673 l_n - 425.362 & th_1 \leq l_n \end{cases}. \tag{4.9}$$

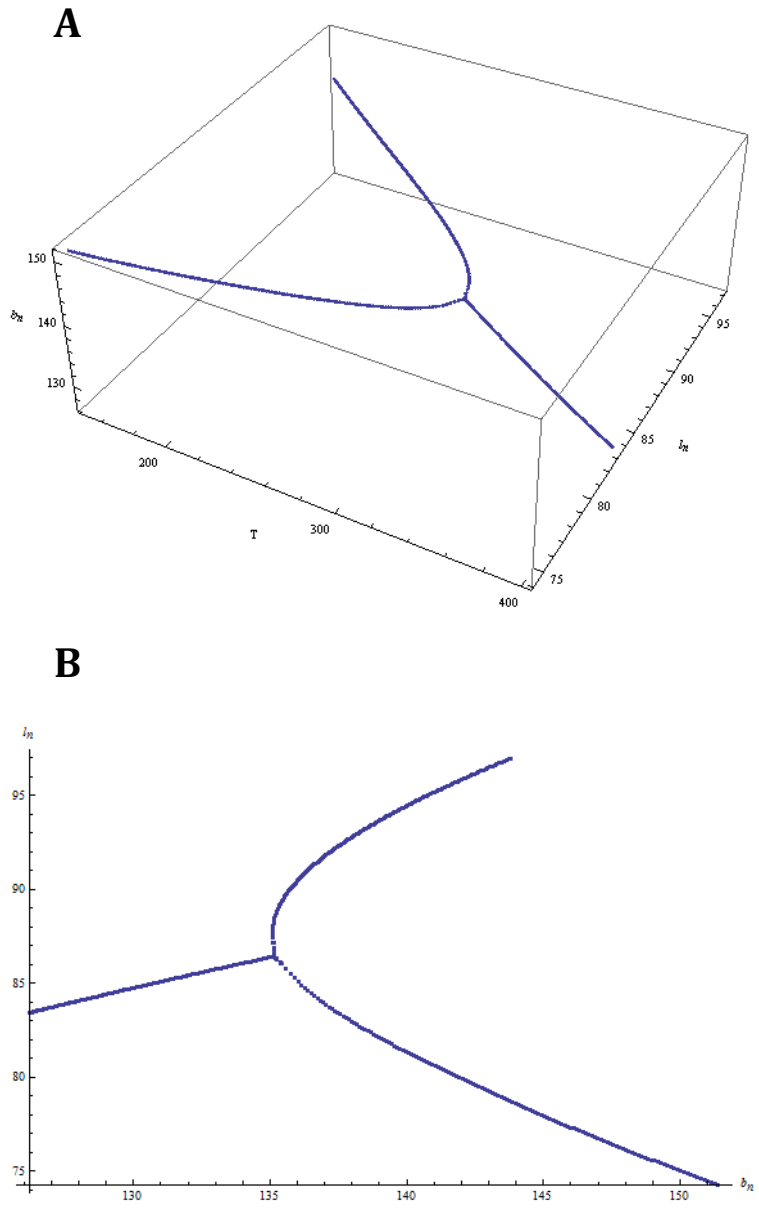

Figure 12 Our original two-dimensional map is plotted here. (A) Bifurcation diagram showing b_n vs. l_n; (B) Bifurcation diagram showing bifurcation with respect to varying parameter T.

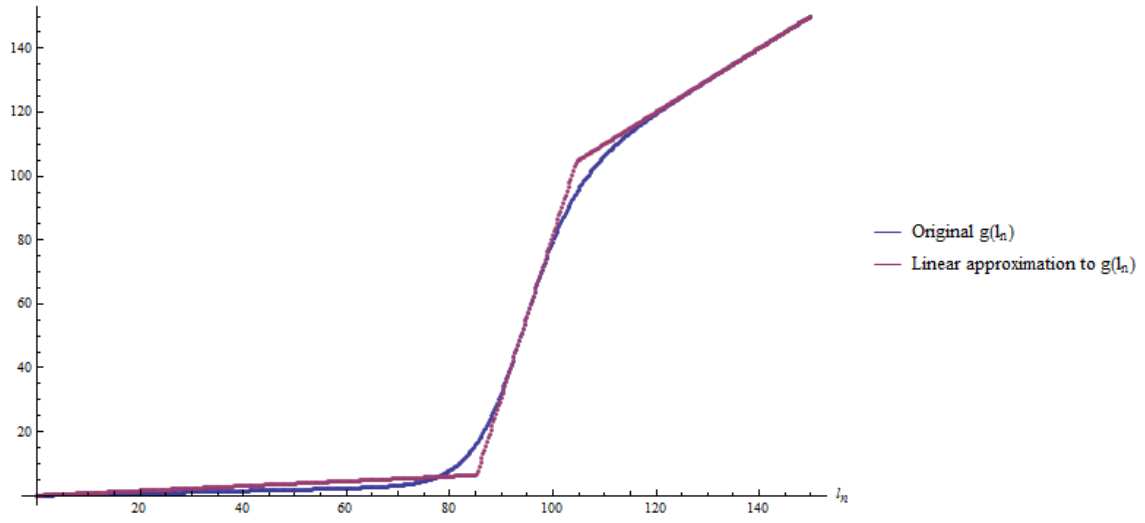

Figure 13 This figure shows a piecewise linear approximation of our function $g(l_n)$ from the text. This approximation uses $l_n = 95$ as a reference point, then calculates the intersections of the line tangent to $g(l_n)$ at $l_n = 95$ and two other predetermined lines. The original function is shown in blue; the approximation is in purple.

We will label

$$g_1(l_n) = \frac{3}{40} l_n,$$

and

$$g_2(l_n) = 5.0673 l_n - 425.362,$$

to which we will refer later. We insert Equation (4.9) into Equation (4.5) to obtain the now piecewise return map:

$$\begin{cases} l_{n+1} = l_n - g_{lin}(l_n) + h\left(c_{n+1}^p\right) \\ b_{n+1} = b_n - \kappa[c_n - c(T)] \end{cases}. \tag{4.10}$$

We use this system of equations to observe our new bifurcation diagram, which is shown in Figure 14. The first thing that we notice in Figure 14 is that our plot seems to have

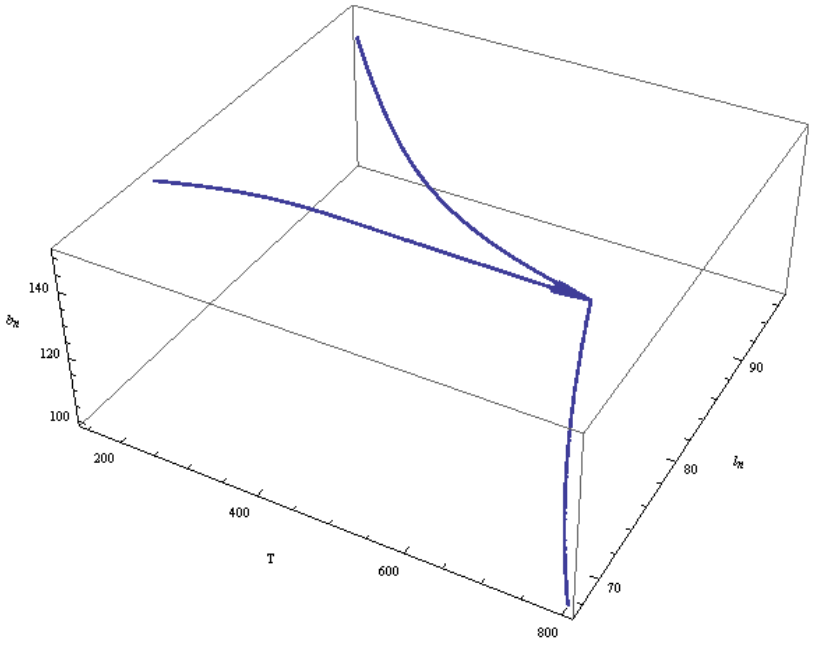

Figure 15 This figure demonstrates our new bifurcation diagram after changing g to a piecewise linear function.

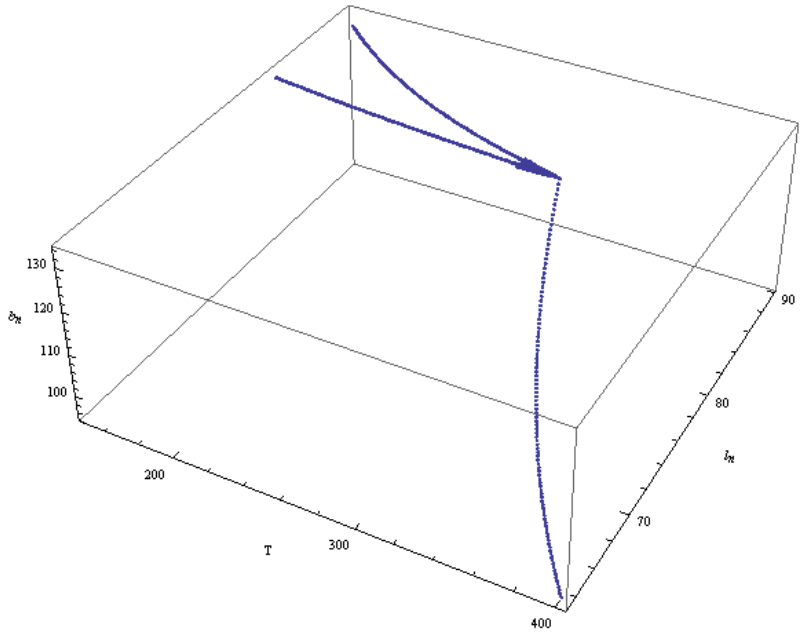

Figure 14 This figure demonstrates our new bifurcation diagram after changing g to a piecewise linear function, and then scaling with respect to T.

shifted due to the linearization of our g function. Therefore, in order to keep consistent with our original model, we rescale our model with respect to T. This transformation will aim to shift our bifurcation point back to approximately 300ms, which is where we started in Figure 12. Thus, we redefine our $c(T)$ function in the following respect:

$$c(T) = 28\left(1 + 2e^{-\frac{\frac{645}{300}T}{300}}\right). \tag{4.11}$$

This rescaling provides us with the plot shown in Figure 15.

Next, we define a linear approximation for our h function. We observe that h is essentially asymptotic to a linear function; however, we observe in our model that c_{n+1}^p largely satisfies $40 \leq c_{n+1}^p \leq 140$. Thus, we derive a strong approximation within this range. We proceed with a similar strategy to that which we utilized in approximating our g function above. We again define a reference point, $c_{n+1}^p = 100$. Next, we calculate the derivative of h at our reference point and find that $h'(100) \approx 0.5099$. We calculate the y-intercept to find our new linear approximation function will be defined to be

$$h_{lin}\left(c_{n+1}^p\right) = 0.5099c_{n+1}^p - 14.0207. \tag{4.12}$$

This approximation is shown in Figure 16, with the original function h shown in blue and the linear approximation h_{lin} shown in purple. We insert Equation (4.12) into our already modified Equation (4.10) to obtain the piecewise return map:

$$\begin{cases} l_{n+1} = l_n - g_{lin}(l_n) + h_{lin}\left(c_{n+1}^p\right) \\ b_{n+1} = b_n - \kappa[c_n - c(T)] \end{cases}. \tag{4.13}$$

Recall c(T) here has been changed to that found in Equation (4.11). However, this previous rescaling attempt shows, in Figure 17, that we did not quite finish with our

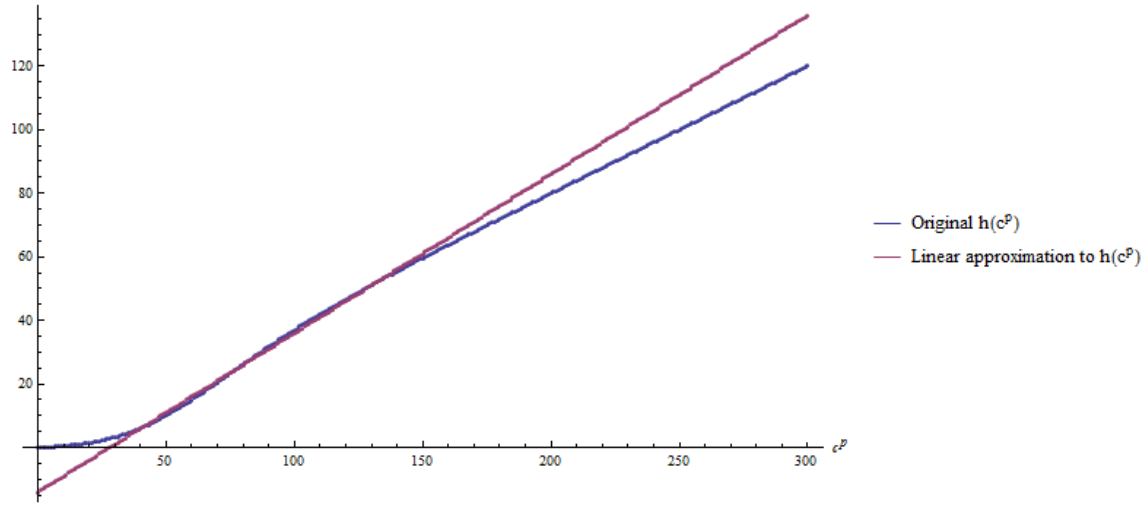

Figure 16 This figure shows a linear approximation of our function $h\left(c_{n+1}^{p}\right)$ from the text. This approximation uses $c_{n+1}^{p} = 100$ as a reference point, then calculates the line tangent to $h\left(c_{n+1}^{p}\right)$ at $c_{n+1}^{p} = 100$. The original function is shown in blue; the approximation is in purple.

rescaling efforts. Once again, we aim to rescale with respect to T so that our bifurcation occurs at approximately 300ms. Thus, our function $c(T)$ becomes

$$c(T) = 28\left(1 + 2e^{-\frac{\left(\frac{645}{300}\right)\left(\frac{320}{300}\right)T}{300}}\right). \tag{4.14}$$

Substituting Equation (4.14) into Equation (4.13) provides us with the results shown in Figure 18.

Lastly, before we proceed to our analysis, we will define a linear map to approximate our newest $c(T)$ function found in Equation (4.14) in order to obtain a true piecewise linear return map. In creating this approximation, we select two reference points, $T = 200$ and $T = 350$, and calculate the values of $c(200)$ and $c(350)$. Then, we derive the line passing through $\big(200, c(200)\big)$ and $\big(350, c(350)\big)$. This process leads us to the linear approximation shown in Figure 19, which is given by the function

$$c_{lin}(T) = -0.0552T + 51.1833. \tag{4.15}$$

When we substitute Equation (4.15) into Equation (4.13), we have a piecewise linear return map, which can be written

$$\begin{cases} l_{n+1} = l_n - g_{lin}(l_n) + h_{lin}\big(c_{n+1}^p\big) \\ b_{n+1} = b_n - \kappa[c_n - c_{lin}(T)] \end{cases}. \tag{4.16}$$

Now we pause to compare our original bifurcation diagram to our result thus far. Notice that, due to our rescaling of c, when we substitute c_{lin} into our system, we still have a bifurcation occurring at approximately $T = 320$ms, which is a fair approximation to our original system. In Figure 20, we show our modified system exactly as it compares

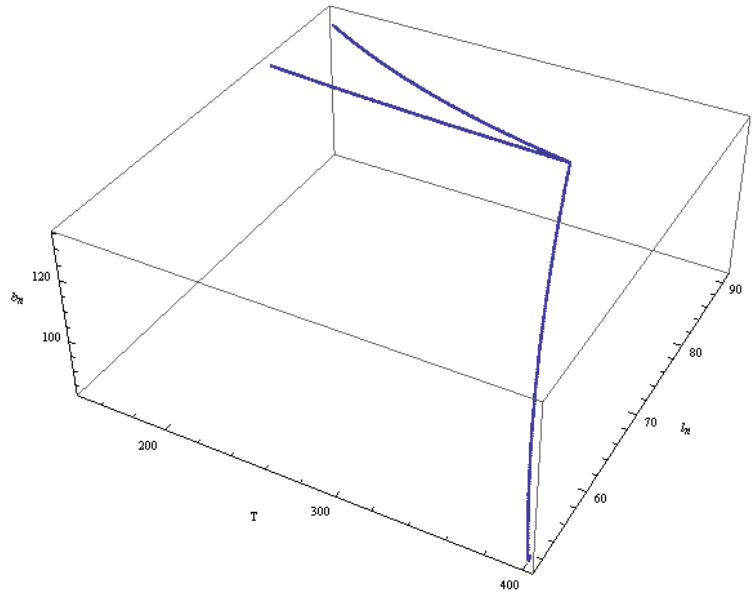

Figure 17 This figure demonstrates our new bifurcation diagram after changing g to a piecewise linear function, rescaling with respect to T, and then changing h to a linear function.

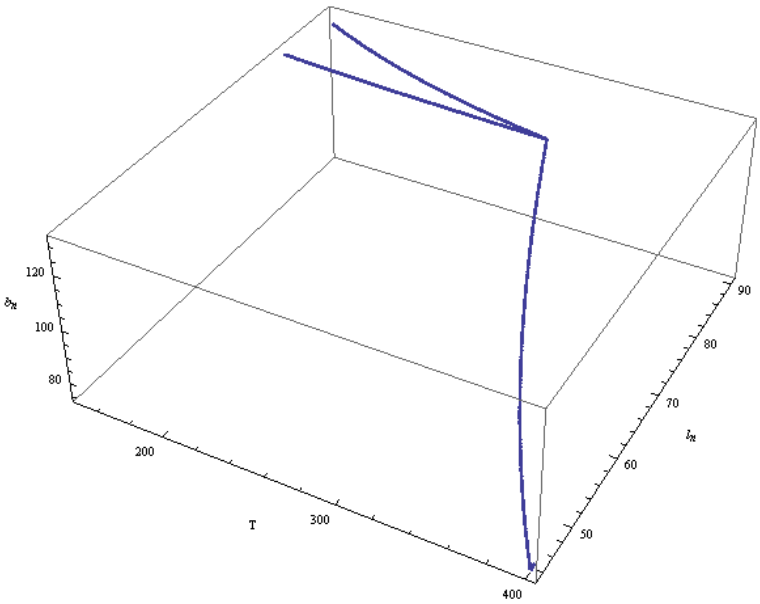

Figure 18 This figure demonstrates our new bifurcation diagram after changing g to a piecewise linear function, rescaling with respect to T, changing h to a linear function, and rescaling with respect to T once more.

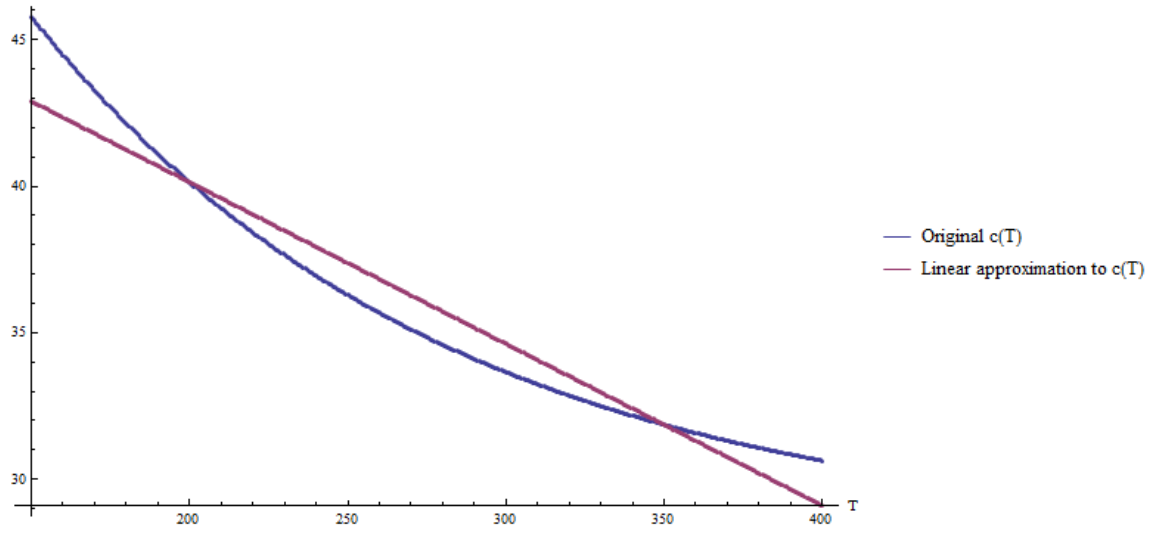

Figure 19 This figure shows a linear approximation of our function $c(T)$ from the text. This approximation uses $T = 200$ and $T = 350$ as reference points, then calculates the line passing through these points. The original function is shown in blue; the approximation is in purple.

to Figure 12, plotting b_n vs. l_n in Figure 20A, and including our parameter T in Figure 20B. Observe now that Figure 20 shows our linear two-dimensional piecewise return map, as desired.

Before continuing, we redefine Equation (4.16) by creating a pure two-dimensional mapping model. Thus, we aim to substitute some combination of l_n and b_n in place of c_{n+1}^p and c_n. We notice, from Chapter 2:

$$c_n = b_n - l_n \tag{4.17}$$

$$c_{n+1}^p = c_n + r_{n+1}. \tag{4.18}$$

In our model, we know that $r_{n+1} = g_{lin}(l_n)$, and so we can substitute Equation (4.17) into Equation (4.18) to see that

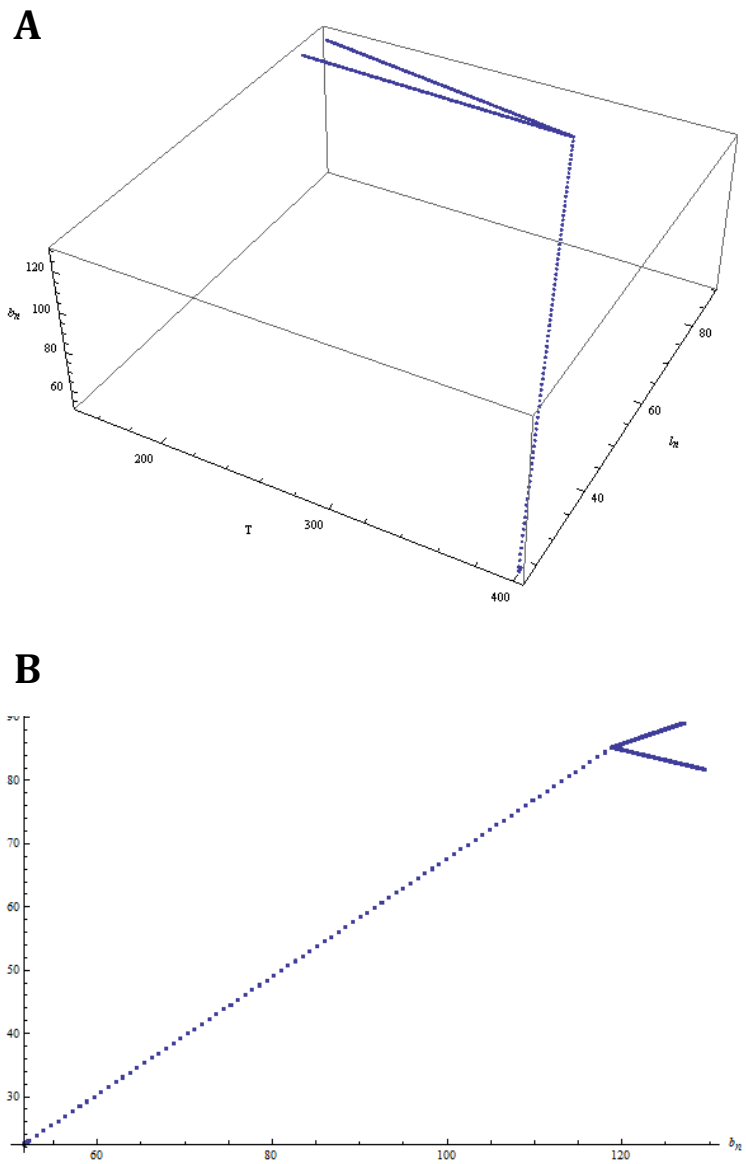

Figure 20 This figure demonstrates our new bifurcation diagrams of our two-dimensional piecewise linear map. This is what occurs after changing g to a piecewise linear function, rescaling with respect to T, changing h to a linear function, and rescaling with respect to T once more, then finally changing $c(T)$ to a linear function as well. (A) Bifurcation diagram showing bifurcation with respect to varying parameter T; (B) Bifurcation diagram showing b_n vs. l_n.

$$c_{n+1}^{p} = b_n - l_n + g_{lin}(l_n).$$

Then, Equation (4.16) becomes:

$$\begin{cases} l_{n+1} = l_n - g_{lin}(l_n) + h_{lin}\big(b_n - l_n + g_{lin}(l_n)\big) \\ b_{n+1} = b_n - \kappa[b_n - l_n - c_{lin}(T)] \end{cases}, \tag{4.19}$$

which is a two-dimensional piecewise linear return map, with varying parameter T.

Now we begin an analysis of this system, similar to that presented in Banerjee et al. [27]. In order to continue with this analysis, we check all of the conditions that must hold. We notice that our map, which we will define to be $G(l_n, b_n; T)$, is indeed a two-dimensional piecewise smooth map and depends on a single parameter T. We seek to define a boundary, denoted Γ_T, given by a smooth curve $l_n = H(b_n; T)$, that divides the phase plane into two regions R_A and R_B. We observe this curve to be given by $l_n = th_1 \approx 85.2$. This map will then be

$$G(l_n, b_n; T) \coloneqq \begin{cases} G_1(l_n, b_n; T) & (l_n, b_n) \epsilon R_A \\ G_2(l_n, b_n; T) & (l_n, b_n) \epsilon R_B \end{cases}. \tag{4.20}$$

Notice that we will write $G(l_n, b_n; T)$ as

$$\begin{pmatrix} l_{n+1} \\ b_{n+1} \end{pmatrix} \coloneqq \begin{cases} \begin{pmatrix} l_n - g_1(l_n) + h_{lin}\big(b_n - l_n + g_1(l_n)\big) \\ b_n - \kappa[b_n - l_n - c_{lin}(T)] \end{pmatrix} & l_n < th_1 \\ \begin{pmatrix} l_n - g_2(l_n) + h_{lin}\big(b_n - l_n + g_2(l_n)\big) \\ b_n - \kappa[b_n - l_n - c_{lin}(T)] \end{pmatrix} & th_1 \leq l_n \end{cases}. \tag{4.21}$$

We observe that the functions defined in Equation (4.21) are both continuous and have continuous derivatives. The map G is continuous as well, with discontinuous derivative at the line Γ_T, which we refer to as the border. The one-sided partial derivatives at Γ_T are finite, and so we have satisfied all of the conditions required to perform our analysis. Now, we aim to study the bifurcations of this system as the parameter T is varied.

A common procedure in studying border-collision bifurcations depends only on the local properties of the map in the neighborhood of the border [27], and so we will study the border-collision bifurcations presented here using normal forms, which is the piecewise affine approximations of G in the neighborhood of the border. We, however, already have affine functions, and so we aim to convert Equation (4.21) into matrix-vector form. First, we will look to expand Equation (4.21), so that we can write it in such a form. By setting $\kappa = 0.5$, Equation (4.21) becomes

$$\begin{pmatrix} l_{n+1} \\ b_{n+1} \end{pmatrix} = \begin{cases} \begin{pmatrix} \frac{37}{40} l_n + h_{lin}\left(b_n - \frac{37}{40} l_n\right) \\ b_n - 0.5[b_n - l_n - c_{lin}(T)] \end{pmatrix} & l_n < th_1 \\ \begin{pmatrix} -4.0673 l_n + 425.362 + h_{lin}(b_n + 4.0673 l_n - 425.362) \\ b_n - 0.5[b_n - l_n - c_{lin}(T)] \end{pmatrix} & th_1 \le l_n \end{cases}$$

$$= \begin{cases} \begin{pmatrix} \frac{37}{40} l_n + 0.5099\left(b_n - \frac{37}{40} l_n\right) - 14.0207 \\ b_n - 0.5[b_n - l_n - c_{lin}(T)] \end{pmatrix} & l_n < th_1 \\ \begin{pmatrix} -4.0673 l_n + 425.362 + 0.5099(b_n + 4.0673 l_n - 425.362) - 14.0207 \\ b_n - 0.5[b_n - l_n - c_{lin}(T)] \end{pmatrix} & th_1 \le l_n \end{cases}$$

$$= \begin{cases} \begin{pmatrix} 0.4534 l_n + 0.5099 b_n - 14.0207 \\ b_n - 0.5[b_n - l_n - c_{lin}(T)] \end{pmatrix} & l_n < th_1 \\ \begin{pmatrix} -1.9934 l_n + 0.5099 b_n + 194.4492 \\ b_n - 0.5[b_n - l_n - c_{lin}(T)] \end{pmatrix} & th_1 \le l_n \end{cases}$$

$$= \begin{cases} \begin{pmatrix} 0.4534 l_n + 0.5099 b_n - 14.0207 \\ 0.5 l_n + 0.5 b_n - 0.0276 T + 25.5917 \end{pmatrix} & l_n < th_1 \\ \begin{pmatrix} -1.9934 l_n + 0.5099 b_n + 194.4492 \\ 0.5 l_n + 0.5 b_n - 0.0276 T + 25.5917 \end{pmatrix} & th_1 \le l_n \end{cases}.$$

Hence, we see that

$$G(l_n, b_n; T) := \begin{cases} \begin{pmatrix} 0.4534 l_n + 0.5099 b_n - 14.0207 \\ 0.5 l_n + 0.5 b_n - 0.0276 T + 25.5917 \end{pmatrix} & l_n < th_1 \\ \begin{pmatrix} -1.9934 l_n + 0.5099 b_n + 194.4492 \\ 0.5 l_n + 0.5 b_n - 0.0276 T + 25.5917 \end{pmatrix} & th_1 \le l_n \end{cases}. \tag{4.22}$$

In order to obtain a normal form for this system, we need to first shift our bifurcation to the origin. Thus, we define $\tilde{l}_n = l_n - H(b_n; T)$, $\tilde{b}_n = b_n$, and so we obtain new variables:

$$\tilde{l}_n = l_n - th_1;\ \tilde{b}_n = b_n.$$

This T-independent change of variables moves the border to the $\tilde{b}_n$-axis. Then the map $G(l_n, b_n; T)$ can be rewritten as

$$G\left(\tilde{l}_n + th_1, \tilde{b}_n; T\right) = F\left(\tilde{l}_n, \tilde{b}_n; T\right),$$

where the border is $\tilde{l}_n = th_1$. We notice that when $T = bif_T \approx 320$, the map $F\left(\tilde{l}_n, \tilde{b}_n; T\right)$ has a fixed point T_0 on the border; that is,

$$T_0 = \left(0, \tilde{b}_n(bif_T)\right) = F\left(0, \tilde{b}_n(bif_T); bif_T\right).$$

Therefore, we claim that a bifurcation occurs at the point $\left(th_1, bif_{b_n}; bif_{\ T}\right)$, and so we implement yet another change of variables to obtain:

$$\begin{cases} \bar{l}_n = \tilde{l}_n; \\ \bar{b}_n = \tilde{b}_n - bif_{b_n}; \\ \bar{T} = T - bif_T. \end{cases}$$

Hence, from where we began to where we are now with our variables, we have:

$$\begin{cases} \bar{l}_n = l_n - th_1; \\ \bar{b}_n = b_n - bif_{b_n}; \\ \bar{T} = T - bif_T. \end{cases}$$

This transformation puts the bifurcation point at the origin; we call this new map $\bar{F}\left(\bar{l}_n, \bar{b}_n; \bar{T}\right)$. Now, for this system to be in normal form, we should have a unit vector in the $\bar{b}_n$ direction map to a unit vector in the $\bar{l}_n$ direction. This fact will provide us with a very simple matrix that we will use to compare traces and determinants of the left side

and right side of the border, now $\bar{l}_n = 0$, which will hopefully shed some light on the border-collision bifurcations that we will obtain from this system.

Before we look at our $\bar{F}$ map, we look at our original G map in matrix-vector form. Notice from Equation (4.22) that we have

$$G(l_n, b_n; T) := \begin{cases} \begin{pmatrix} 0.4534l_n + 0.5099b_n - 14.0207 \\ 0.5l_n + 0.5b_n - 0.0276T + 25.5917 \end{pmatrix} & l_n < th_1 \\ \begin{pmatrix} -1.9934l_n + 0.5099b_n + 194.4492 \\ 0.5l_n + 0.5b_n - 0.0276T + 25.5917 \end{pmatrix} & th_1 \leq l_n \end{cases},$$

so that

$$(4.23)\ \begin{pmatrix} l_{n+1} \\ b_{n+1} \end{pmatrix} = \begin{cases} \begin{pmatrix} 0.4534 & 0.5099 \\ 0.5 & 0.5 \end{pmatrix} \begin{pmatrix} l_n \\ b_n \end{pmatrix} + T \begin{pmatrix} 0 \\ -0.0276 \end{pmatrix} + \begin{pmatrix} -14.0207 \\ 25.5917 \end{pmatrix} & l_n < th_1 \\ \begin{pmatrix} -1.9934 & 0.5099 \\ 0.5 & 0.5 \end{pmatrix} \begin{pmatrix} l_n \\ b_n \end{pmatrix} + T \begin{pmatrix} 0 \\ -0.0276 \end{pmatrix} + \begin{pmatrix} 194.4492 \\ 25.5917 \end{pmatrix} & th_1 \leq l_n \end{cases}$$

From Equation (4.23) above, we perform transformations to our variables to obtain:

$$\begin{pmatrix} \bar{l}_{n+1} + th_1 \\ \bar{b}_{n+1} + bif_{b_n} \end{pmatrix}$$

$$= \begin{cases} \begin{pmatrix} 0.4534 & 0.5099 \\ 0.5 & 0.5 \end{pmatrix} \begin{pmatrix} \bar{l}_n + th_1 \\ \bar{b}_n + bif_{b_n} \end{pmatrix} + T \begin{pmatrix} 0 \\ -0.0276 \end{pmatrix} + \begin{pmatrix} -14.0207 \\ 25.5917 \end{pmatrix} & \bar{l}_n < 0 \\ \begin{pmatrix} -1.9934 & 0.5099 \\ 0.5 & 0.5 \end{pmatrix} \begin{pmatrix} \bar{l}_n + th_1 \\ \bar{b}_n + bif_{b_n} \end{pmatrix} + T \begin{pmatrix} 0 \\ -0.0276 \end{pmatrix} + \begin{pmatrix} 194.4492 \\ 25.5917 \end{pmatrix} & 0 \leq \bar{l}_n \end{cases}$$

$$= \begin{cases} \begin{pmatrix} 0.4534 & 0.5099 \\ 0.5 & 0.5 \end{pmatrix} \begin{pmatrix} \bar{l}_n \\ \bar{b}_n \end{pmatrix} + \begin{pmatrix} 0.4534 & 0.5099 \\ 0.5 & 0.5 \end{pmatrix} \begin{pmatrix} th_1 \\ bif_{b_n} \end{pmatrix} & \bar{l}_n < 0 \\ \quad + T \begin{pmatrix} 0 \\ -0.0276 \end{pmatrix} + \begin{pmatrix} -14.0207 \\ 25.5917 \end{pmatrix} & \\ \begin{pmatrix} -1.9934 & 0.5099 \\ 0.5 & 0.5 \end{pmatrix} \begin{pmatrix} \bar{l}_n \\ \bar{b}_n \end{pmatrix} + \begin{pmatrix} -1.9934 & 0.5099 \\ 0.5 & 0.5 \end{pmatrix} \begin{pmatrix} th_1 \\ bif_{b_n} \end{pmatrix} & 0 \leq \bar{l}_n \\ \quad + T \begin{pmatrix} 0 \\ -0.0276 \end{pmatrix} + \begin{pmatrix} 194.4492 \\ 25.5917 \end{pmatrix} & \end{cases}$$

$$= \begin{cases} \begin{pmatrix} 0.4534 & 0.5099 \\ 0.5 & 0.5 \end{pmatrix} \begin{pmatrix} \bar{l}_n \\ \bar{b}_n \end{pmatrix} + \begin{pmatrix} 0.4534 & 0.5099 \\ 0.5 & 0.5 \end{pmatrix} \begin{pmatrix} th_1 \\ bif_{b_n} \end{pmatrix} & \bar{l}_n < 0 \\ +(T - bif_T) \begin{pmatrix} 0 \\ -0.0276 \end{pmatrix} + bif_T \begin{pmatrix} 0 \\ -0.0276 \end{pmatrix} + \begin{pmatrix} -14.0207 \\ 25.5917 \end{pmatrix} & \\ \begin{pmatrix} -1.9934 & 0.5099 \\ 0.5 & 0.5 \end{pmatrix} \begin{pmatrix} \bar{l}_n \\ \bar{b}_n \end{pmatrix} + \begin{pmatrix} -1.9934 & 0.5099 \\ 0.5 & 0.5 \end{pmatrix} \begin{pmatrix} th_1 \\ bif_{b_n} \end{pmatrix} & 0 \le \bar{l}_n \\ +(T - bif_T) \begin{pmatrix} 0 \\ -0.0276 \end{pmatrix} + bif_T \begin{pmatrix} 0 \\ -0.0276 \end{pmatrix} + \begin{pmatrix} 194.4492 \\ 25.5917 \end{pmatrix} & \end{cases}$$

$$= \begin{cases} \begin{pmatrix} 0.4534 & 0.5099 \\ 0.5 & 0.5 \end{pmatrix} \begin{pmatrix} \bar{l}_n \\ \bar{b}_n \end{pmatrix} + \begin{pmatrix} 0.4534 & 0.5099 \\ 0.5 & 0.5 \end{pmatrix} \begin{pmatrix} th_1 \\ bif_{b_n} \end{pmatrix} & \bar{l}_n < 0 \\ +\bar{T} \begin{pmatrix} 0 \\ -0.0276 \end{pmatrix} + bif_T \begin{pmatrix} 0 \\ -0.0276 \end{pmatrix} + \begin{pmatrix} -14.0207 \\ 25.5917 \end{pmatrix} & \\ \begin{pmatrix} -1.9934 & 0.5099 \\ 0.5 & 0.5 \end{pmatrix} \begin{pmatrix} \bar{l}_n \\ \bar{b}_n \end{pmatrix} + \begin{pmatrix} -1.9934 & 0.5099 \\ 0.5 & 0.5 \end{pmatrix} \begin{pmatrix} th_1 \\ bif_{b_n} \end{pmatrix} & 0 \le \bar{l}_n \\ +\bar{T} \begin{pmatrix} 0 \\ -0.0276 \end{pmatrix} + bif_T \begin{pmatrix} 0 \\ -0.0276 \end{pmatrix} + \begin{pmatrix} 194.4492 \\ 25.5917 \end{pmatrix} & \end{cases}$$

Therefore, we have

$$\begin{pmatrix} \bar{l}_{n+1} \\ \bar{b}_{n+1} \end{pmatrix}$$

$$= \begin{cases} \begin{pmatrix} 0.4534 & 0.5099 \\ 0.5 & 0.5 \end{pmatrix} \begin{pmatrix} \bar{l}_n \\ \bar{b}_n \end{pmatrix} + \begin{pmatrix} 0.4534 & 0.5099 \\ 0.5 & 0.5 \end{pmatrix} \begin{pmatrix} th_1 \\ bif_{b_n} \end{pmatrix} - \begin{pmatrix} th_1 \\ bif_{b_n} \end{pmatrix} & \bar{l}_n < 0 \\ +\bar{T} \begin{pmatrix} 0 \\ -0.0276 \end{pmatrix} + bif_T \begin{pmatrix} 0 \\ -0.0276 \end{pmatrix} + \begin{pmatrix} -14.0207 \\ 25.5917 \end{pmatrix} & \\ \begin{pmatrix} -1.9934 & 0.5099 \\ 0.5 & 0.5 \end{pmatrix} \begin{pmatrix} \bar{l}_n \\ \bar{b}_n \end{pmatrix} + \begin{pmatrix} -1.9934 & 0.5099 \\ 0.5 & 0.5 \end{pmatrix} \begin{pmatrix} th_1 \\ bif_{b_n} \end{pmatrix} - \begin{pmatrix} th_1 \\ bif_{b_n} \end{pmatrix} & 0 \le \bar{l}_n \\ +\bar{T} \begin{pmatrix} 0 \\ -0.0276 \end{pmatrix} + bif_T \begin{pmatrix} 0 \\ -0.0276 \end{pmatrix} + \begin{pmatrix} 194.4492 \\ 25.5917 \end{pmatrix} & \end{cases}$$

$$= \begin{cases} \begin{pmatrix} 0.4534 & 0.5099 \\ 0.5 & 0.5 \end{pmatrix} \begin{pmatrix} \bar{l}_n \\ \bar{b}_n \end{pmatrix} + \bar{T} \begin{pmatrix} 0 \\ -0.0276 \end{pmatrix} + bif_T \begin{pmatrix} 0 \\ -0.0276 \end{pmatrix} & \bar{l}_n < 0 \\ + \begin{pmatrix} 0.4534 & 0.5099 \\ 0.5 & 0.5 \end{pmatrix} \begin{pmatrix} th_1 \\ bif_{b_n} \end{pmatrix} - \begin{pmatrix} th_1 \\ bif_{b_n} \end{pmatrix} + \begin{pmatrix} -14.0207 \\ 25.5917 \end{pmatrix} & \\ \begin{pmatrix} -1.9934 & 0.5099 \\ 0.5 & 0.5 \end{pmatrix} \begin{pmatrix} \bar{l}_n \\ \bar{b}_n \end{pmatrix} + \bar{T} \begin{pmatrix} 0 \\ -0.0276 \end{pmatrix} + bif_T \begin{pmatrix} 0 \\ -0.0276 \end{pmatrix} & 0 \le \bar{l}_n \\ + \begin{pmatrix} -1.9934 & 0.5099 \\ 0.5 & 0.5 \end{pmatrix} \begin{pmatrix} th_1 \\ bif_{b_n} \end{pmatrix} - \begin{pmatrix} th_1 \\ bif_{b_n} \end{pmatrix} + \begin{pmatrix} 194.4492 \\ 25.5917 \end{pmatrix} & \end{cases}.$$

However, since

$$bif_T\begin{pmatrix}0\\-0.0276\end{pmatrix}+\begin{pmatrix}0.4534 & 0.5099\\0.5 & 0.5\end{pmatrix}\begin{pmatrix}th_1\\bif_{b_n}\end{pmatrix}-\begin{pmatrix}th_1\\bif_{b_n}\end{pmatrix}+\begin{pmatrix}-14.0207\\25.5917\end{pmatrix}=0$$

and

$$bif_T\begin{pmatrix}0\\-0.0276\end{pmatrix}+\begin{pmatrix}-1.9934 & 0.5099\\0.5 & 0.5\end{pmatrix}\begin{pmatrix}th_1\\bif_{b_n}\end{pmatrix}-\begin{pmatrix}th_1\\bif_{b_n}\end{pmatrix}+\begin{pmatrix}194.4492\\25.5917\end{pmatrix}=0,$$

we see that our return map $\bar{F}$ becomes

$$\bar{F}(\bar{l}_n,\bar{b}_n;\bar{T}) \coloneqq \begin{cases}\begin{pmatrix}0.4534 & 0.5099\\0.5 & 0.5\end{pmatrix}\begin{pmatrix}\bar{l}_n\\\bar{b}_n\end{pmatrix}+\bar{T}\begin{pmatrix}0\\-0.0276\end{pmatrix} & \bar{l}_n<0\\ \begin{pmatrix}-1.9934 & 0.5099\\0.5 & 0.5\end{pmatrix}\begin{pmatrix}\bar{l}_n\\\bar{b}_n\end{pmatrix}+\bar{T}\begin{pmatrix}0\\-0.0276\end{pmatrix} & 0\le\bar{l}_n\end{cases}. \tag{4.24}$$

We can use this Equation (4.24) to observe the bifurcation phenomenon around the origin, as shown in Figure 21. Notice that the border-collision bifurcation has not changed in any regard, except that it has been shifted to the origin rather than at our original bifurcation point.

Because our goal is to turn this system into normal form, we need to perform a linear transformation on $\bar{F}$ so that it takes the form:

$$G_2(x_n,y_n;\mu) \coloneqq \begin{cases}\begin{pmatrix}\tau_L & 1\\-\delta_L & 0\end{pmatrix}\begin{pmatrix}x_n\\y_n\end{pmatrix}+\mu\begin{pmatrix}1\\0\end{pmatrix} & x_n<0\\ \begin{pmatrix}\tau_R & 1\\-\delta_R & 0\end{pmatrix}\begin{pmatrix}x_n\\y_n\end{pmatrix}+\mu\begin{pmatrix}1\\0\end{pmatrix} & 0\le x_n\end{cases}.$$

Therefore, we aim to find a matrix $\mathcal{L}$ such that the following transformation holds:

$$\begin{pmatrix}\bar{x}_n\\\bar{y}_n\end{pmatrix}=\mathcal{L}\begin{pmatrix}\bar{l}_n\\\bar{b}_n\end{pmatrix}.$$

This would allow

$$\begin{pmatrix}\bar{x}_{n+1}\\\bar{y}_{n+1}\end{pmatrix}=\mathcal{L}\begin{pmatrix}\bar{l}_{n+1}\\\bar{b}_{n+1}\end{pmatrix}$$

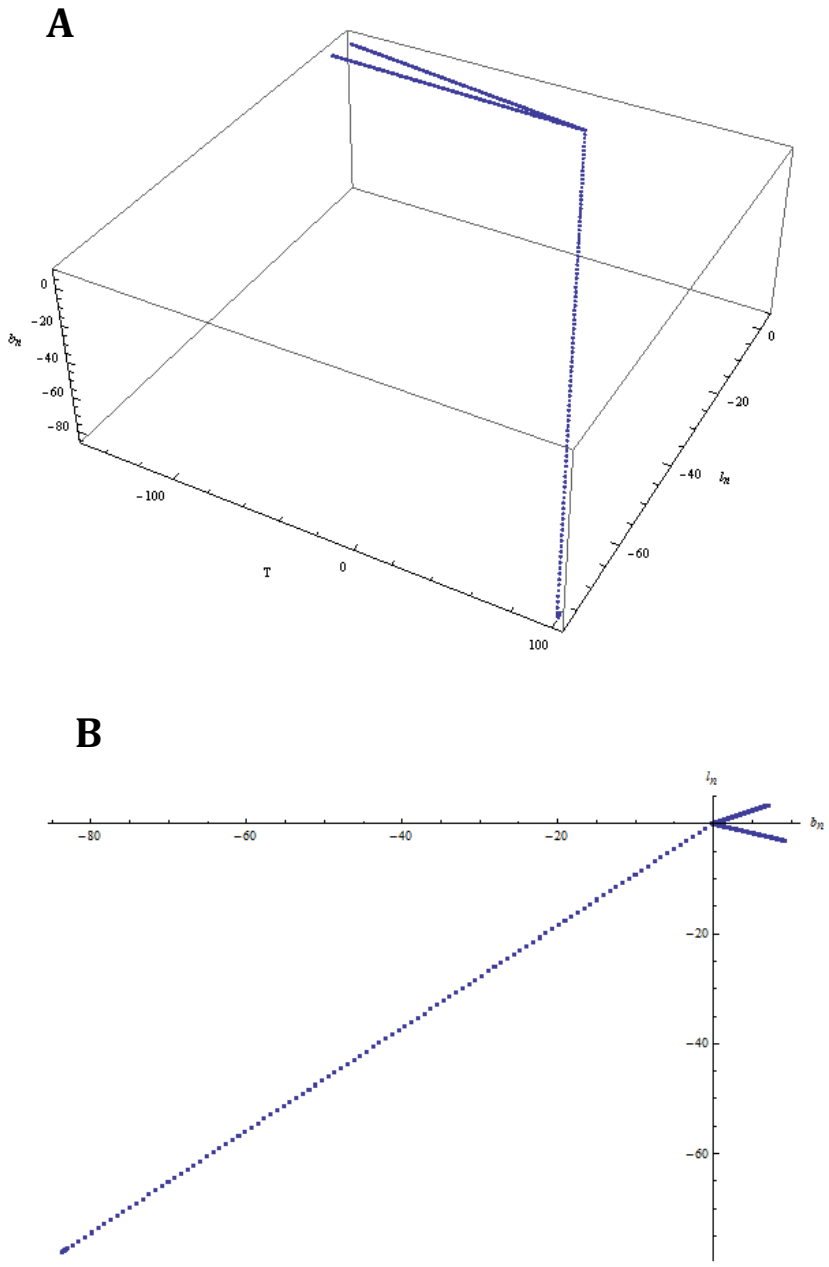

Figure 21 This figure demonstrates our new, translated bifurcation diagrams of our two-dimensional piecewise linear map. This is what occurs after changing g to a piecewise linear function, rescaling with respect to T, changing h to a linear function, and rescaling with respect to T once more, changing $c(T)$ to a linear function as well, and finally shifting the bifurcation point to the origin. (A) Bifurcation diagram showing bifurcation with respect to varying parameter T; (B) Bifurcation diagram showing b_n vs. l_n.

$$= \begin{cases} \mathcal{L}\begin{pmatrix} 0.4534 & 0.5099 \\ 0.5 & 0.5 \end{pmatrix}\begin{pmatrix} \bar{l}_n \\ \bar{b}_n \end{pmatrix} + \mathcal{L}\bar{T}\begin{pmatrix} 0 \\ -0.0276 \end{pmatrix} & \bar{l}_n < 0 \\ \mathcal{L}\begin{pmatrix} -1.9934 & 0.5099 \\ 0.5 & 0.5 \end{pmatrix}\begin{pmatrix} \bar{l}_n \\ \bar{b}_n \end{pmatrix} + \mathcal{L}\bar{T}\begin{pmatrix} 0 \\ -0.0276 \end{pmatrix} & 0 \leq \bar{l}_n \end{cases}$$

$$= \begin{cases} \mathcal{L}\begin{pmatrix} 0.4534 & 0.5099 \\ 0.5 & 0.5 \end{pmatrix}\mathcal{L}^{-1}\mathcal{L}\begin{pmatrix} \bar{l}_n \\ \bar{b}_n \end{pmatrix} + \bar{T}\mathcal{L}\begin{pmatrix} 0 \\ -0.0276 \end{pmatrix} & \bar{l}_n < 0 \\ \mathcal{L}\begin{pmatrix} -1.9934 & 0.5099 \\ 0.5 & 0.5 \end{pmatrix}\mathcal{L}^{-1}\mathcal{L}\begin{pmatrix} \bar{l}_n \\ \bar{b}_n \end{pmatrix} + \bar{T}\mathcal{L}\begin{pmatrix} 0 \\ -0.0276 \end{pmatrix} & 0 \leq \bar{l}_n \end{cases}$$

$$= \begin{cases} \mathcal{L}\begin{pmatrix} 0.4534 & 0.5099 \\ 0.5 & 0.5 \end{pmatrix}\mathcal{L}^{-1}\left(\mathcal{L}\begin{pmatrix} \bar{l}_n \\ \bar{b}_n \end{pmatrix}\right) + \bar{T}\mathcal{L}\begin{pmatrix} 0 \\ -0.0276 \end{pmatrix} & \bar{l}_n < 0 \\ \mathcal{L}\begin{pmatrix} -1.9934 & 0.5099 \\ 0.5 & 0.5 \end{pmatrix}\mathcal{L}^{-1}\left(\mathcal{L}\begin{pmatrix} \bar{l}_n \\ \bar{b}_n \end{pmatrix}\right) + \bar{T}\mathcal{L}\begin{pmatrix} 0 \\ -0.0276 \end{pmatrix} & 0 \leq \bar{l}_n \end{cases}.$$

Thus, we have

$$\begin{pmatrix} \bar{x}_{n+1} \\ \bar{y}_{n+1} \end{pmatrix} = \begin{cases} \mathcal{L}\begin{pmatrix} 0.4534 & 0.5099 \\ 0.5 & 0.5 \end{pmatrix}\mathcal{L}^{-1}\begin{pmatrix} \bar{x}_n \\ \bar{y}_n \end{pmatrix} + \bar{T}\mathcal{L}\begin{pmatrix} 0 \\ -0.0276 \end{pmatrix} & \bar{x}_n < 0 \\ \mathcal{L}\begin{pmatrix} -1.9934 & 0.5099 \\ 0.5 & 0.5 \end{pmatrix}\mathcal{L}^{-1}\begin{pmatrix} \bar{x}_n \\ \bar{y}_n \end{pmatrix} + \bar{T}\mathcal{L}\begin{pmatrix} 0 \\ -0.0276 \end{pmatrix} & 0 \leq \bar{x}_n \end{cases}. \quad (4.25)$$

Now, we find $\mathcal{L}$ so that

$$\mathcal{L}\begin{pmatrix} 0.4534 & 0.5099 \\ 0.5 & 0.5 \end{pmatrix}\mathcal{L}^{-1} = \begin{pmatrix} \tau_L & 1 \\ -\delta_L & 0 \end{pmatrix},$$

and

$$\mathcal{L}\begin{pmatrix} -1.9934 & 0.5099 \\ 0.5 & 0.5 \end{pmatrix}\mathcal{L}^{-1} = \begin{pmatrix} \tau_R & 1 \\ -\delta_R & 0 \end{pmatrix}.$$

Notice, then, that when $\mathcal{L} = \begin{pmatrix} L_{11} & L_{12} \\ L_{21} & L_{22} \end{pmatrix}$ and $\mathcal{L}^{-1} = \frac{1}{L_{11}L_{22} - L_{12}L_{21}}\begin{pmatrix} L_{22} & -L_{12} \\ -L_{21} & L_{11} \end{pmatrix}$, we have a system of four equations with four unknowns. Our system of equations to solve becomes:

$$\begin{cases} \frac{1}{L_{11}L_{22}-L_{21}L_{12}}\left(-L_{21}(0.4534L_{11}+0.5L_{12})+L_{11}(0.5099L_{11}+0.5L_{12})\right)=1 \\ \frac{1}{L_{11}L_{22}-L_{21}L_{12}}\left(-L_{12}(0.4534L_{21}+0.5L_{22})+L_{11}(0.5099L_{21}+0.5L_{22})\right)=0 \\ \frac{1}{L_{11}L_{22}-L_{21}L_{12}}\left(-L_{21}(-1.9934L_{11}+0.5L_{12})+L_{11}(0.5099L_{11}+0.5L_{12})\right)=1 \\ \frac{1}{L_{11}L_{22}-L_{21}L_{12}}\left(-L_{12}(-1.9934L_{21}+0.5L_{22})+L_{11}(0.5099L_{21}+0.5L_{22})\right)=0 \end{cases}.$$

This becomes

$$\begin{cases} -L_{21}(0.4534L_{11}+0.5L_{12})+L_{11}(0.5099L_{11}+0.5L_{12})=L_{11}L_{22}-L_{21}L_{12} \\ -L_{12}(0.4534L_{21}+0.5L_{22})+L_{11}(0.5099L_{21}+0.5L_{22})=0 \\ -L_{21}(-1.9934L_{11}+0.5L_{12})+L_{11}(0.5099L_{11}+0.5L_{12})=L_{11}L_{22}-L_{21}L_{12} \\ -L_{12}(-1.9934L_{21}+0.5L_{22})+L_{11}(0.5099L_{21}+0.5L_{22})=0 \end{cases}.$$

In solving this system of equations, we find that there are infinitely many solutions, dependent on L_{11}. The solution to this system is given by

$$\begin{cases} L_{11}=L_{11} \\ L_{12}=0 \\ L_{21}=-0.5L_{11} \\ L_{22}=0.5099L_{11} \end{cases}.$$

By defining $L_{11}=1$, we find the matrix $\mathcal{L}$ to be

$$\mathcal{L}=\begin{pmatrix} 1 & 0 \\ -0.5 & 0.5099 \end{pmatrix}.$$

Therefore, we see that our Equation (4.25) has been transformed to become

$$\begin{pmatrix} \bar{x}_{n+1} \\ \bar{y}_{n+1} \end{pmatrix}=\begin{cases} \begin{pmatrix} 0.9534 & 1 \\ 0.02825 & 0 \end{pmatrix}\begin{pmatrix} \bar{x}_n \\ \bar{y}_n \end{pmatrix}+\bar{T}\begin{pmatrix} 0 \\ -0.0141 \end{pmatrix} & \bar{x}_n<0 \\ \begin{pmatrix} -1.4934 & 1 \\ 1.25165 & 0 \end{pmatrix}\begin{pmatrix} \bar{x}_n \\ \bar{y}_n \end{pmatrix}+\bar{T}\begin{pmatrix} 0 \\ -0.0141 \end{pmatrix} & 0\le\bar{x}_n \end{cases}. \tag{4.26}$$

Hence, we have

$$\begin{cases} \tau_L=0.9534 \\ \delta_L=-0.02825 \\ \tau_R=-1.4934 \\ \delta_R=-1.25165 \end{cases} \tag{4.27}$$

Recall that our goal is to transform our system into the form

$$G_2(x_n, y_n; \mu) \coloneqq \begin{cases} \begin{pmatrix} \tau_L & 1 \\ -\delta_L & 0 \end{pmatrix} \begin{pmatrix} x_n \\ y_n \end{pmatrix} + \mu \begin{pmatrix} 1 \\ 0 \end{pmatrix} & x_n < 0 \\ \begin{pmatrix} \tau_R & 1 \\ -\delta_R & 0 \end{pmatrix} \begin{pmatrix} x_n \\ y_n \end{pmatrix} + \mu \begin{pmatrix} 1 \\ 0 \end{pmatrix} & 0 \leq x_n \end{cases}.$$

Therefore, in order to transform this $\bar{F}$ into normal form, we perform a final change of variables to our Equation (4.26), given by

$$\begin{cases} x_n = \bar{x}_n \\ y_n = \bar{y}_n + 0.0141\bar{T}. \\ \mu = -0.0141\bar{T} \end{cases}$$

This will provide us with the new map:

$$\begin{pmatrix} x_{n+1} \\ y_{n+1} \end{pmatrix} = G_2(x_n, y_n; \mu) \coloneqq \begin{cases} \begin{pmatrix} 0.9534 & 1 \\ 0.02825 & 0 \end{pmatrix} \begin{pmatrix} x_n \\ y_n \end{pmatrix} + \mu \begin{pmatrix} 1 \\ 0 \end{pmatrix} & x_n < 0 \\ \begin{pmatrix} -1.4934 & 1 \\ 1.25165 & 0 \end{pmatrix} \begin{pmatrix} x_n \\ y_n \end{pmatrix} + \mu \begin{pmatrix} 1 \\ 0 \end{pmatrix} & 0 \leq x_n \end{cases}, \quad (4.28)$$

which is indeed the normal form of our original piecewise linear map. Notice, as shown in Figure 22, that putting our system into normal form switches the bifurcation direction. Recall, however, from the previous chapter that our bifurcation is invariant under this change. The traces and determinants shown above will provide us information regarding the type of border-collision bifurcation to expect. We refer to Banerjee et al. [27] to gain insight into our anticipated bifurcation.

According to this text, we first examine the determinants of the left and right sides, δ_L and δ_R, respectively. Observe from (4.27) above that both of our determinants are negative. This implies that the eigenvalues are both real for all values of τ_L and τ_R [27], more specifically for $\tau_L = 0.9534$ and $\tau_R = -1.4934$, as in this case. Therefore, there can be no coexisting attractors anywhere in the parameter space. We also know from [27] that the region of stability of the period-2 attractor is given by the conditions

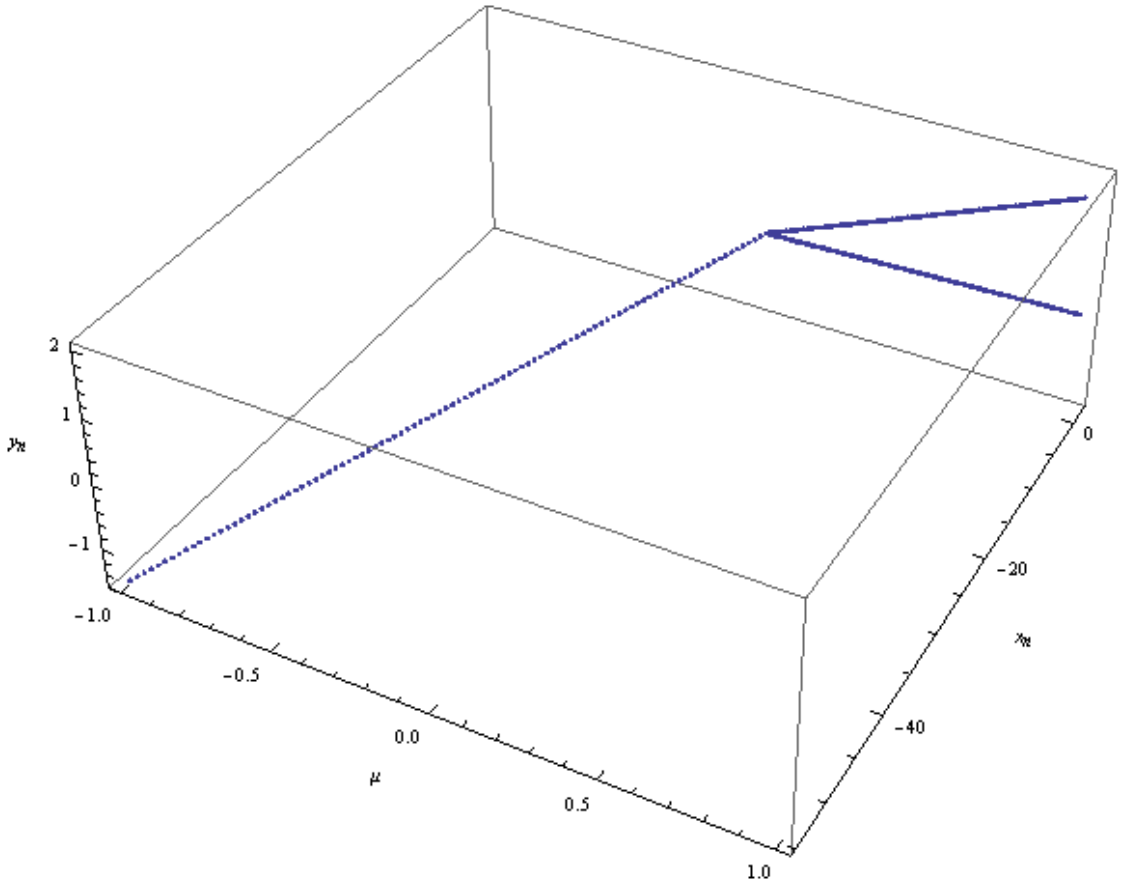

Figure 22 The normalized version of our two-dimensional piecewise return map. Notice the bifurcation occurs at the origin. We also notice that the bifurcation changes from being right-to-left to left-to-right when it takes this normal form.

$$(4.29) \qquad 1 - \tau_L \tau_R + \delta_L + \delta_R + \delta_L \delta_R > 0$$

for $\lambda_1 < 1$ and

$$(4.30) \qquad 1 + \tau_L \tau_R - \delta_L - \delta_R + \delta_L \delta_R > 0$$

for $\lambda_2 > -1$. These are readily satisfied as follows:

$$1 - (0.9534)(-1.4934) + (-0.02825) + (-1.25165) + (-0.02825)(-1.25165)$$
$$= 1.1783 > 0,$$

satisfying condition (4.29), and

$$1 + (0.9534)(-1.4934) - (-0.02825) - (-1.25165) + (-0.02825)(-1.25165)$$
$$= 0.8915 > 0,$$

which satisfies condition (4.30). Therefore, we can expect to observe a period-1 attractor bifurcating into a period-2 response as our plot crosses the threshold $\mu = 0$, as we observe in Figure 22.

Now we want to observe some different results based on the theoretical analysis of Banerjee et al. [27]. According to this study, we will observe a period-1 to period-2 response when the determinants are both negative, and conditions (4.29) and (4.30) are satisfied. Thus, we observe what results when one of these is not satisfied. Let us define

$$(4.31) \qquad \begin{cases} \tau_L = 0.5534 \\ \delta_L = -0.02825 \\ \tau_R = -5.4934 \\ \delta_R = -0.25165 \end{cases}.$$

Then we would have the following system in normal form:

$$(4.32) \qquad G_2(x_n, y_n; \mu) \coloneqq \begin{cases} \begin{pmatrix} 0.5534 & 1 \\ 0.02825 & 0 \end{pmatrix} \begin{pmatrix} x_n \\ y_n \end{pmatrix} + \mu \begin{pmatrix} 1 \\ 0 \end{pmatrix} & x_n < 0 \\ \begin{pmatrix} -5.4934 & 1 \\ 0.25165 & 0 \end{pmatrix} \begin{pmatrix} x_n \\ y_n \end{pmatrix} + \mu \begin{pmatrix} 1 \\ 0 \end{pmatrix} & 0 \leq x_n \end{cases}.$$

We notice that both determinants are still negative, and so we would expect a period-1 to period-2 response as long as conditions (4.29) and (4.30) are satisfied, while we can expect chaos otherwise. We check these conditions:

$$1 - (0.5534)(-5.4934) + (-0.02825) + (-0.25165) + (-0.02825)(-0.25165)$$
$$= 3.7673 > 0,$$

satisfying condition (4.29). However, when we examine condition (4.30), we see

$$1 + (0.5534)(-5.4934) - (-0.02825) - (-0.25165) + (-0.02825)(-0.25165)$$
$$= -1.7530 < 0,$$

so that condition (4.30) is not satisfied. This results in Figure 23, which shows chaos, as we would expect.

Thus, we see results that were predicted in the theoretical study by Banerjee et al. [27] when we keep negative determinants. Now we are interested in what results if we were to obtain positive determinants in our system. Banerjee et al. [27] show a variety of possible results when we have positive determinants. The parameter plot that was proposed in this study is shown in Figure 24. Notice from this plot that if we fix our determinants to be positive, we will obtain these different results by varying the values of τ_L and τ_R, or the left and right traces. Therefore, we set our determinants to be

$$(4.33) \qquad \begin{cases} \delta_L = 0.02825 \\ \delta_R = 0.55165 \end{cases}.$$

The first result that we hope to obtain is shown in region 1a in Figure 24. This region should produce no attractor to a period-1 attractor. We see, then, that

$$1.02825 = 1 + \delta_L < \tau_L$$

and

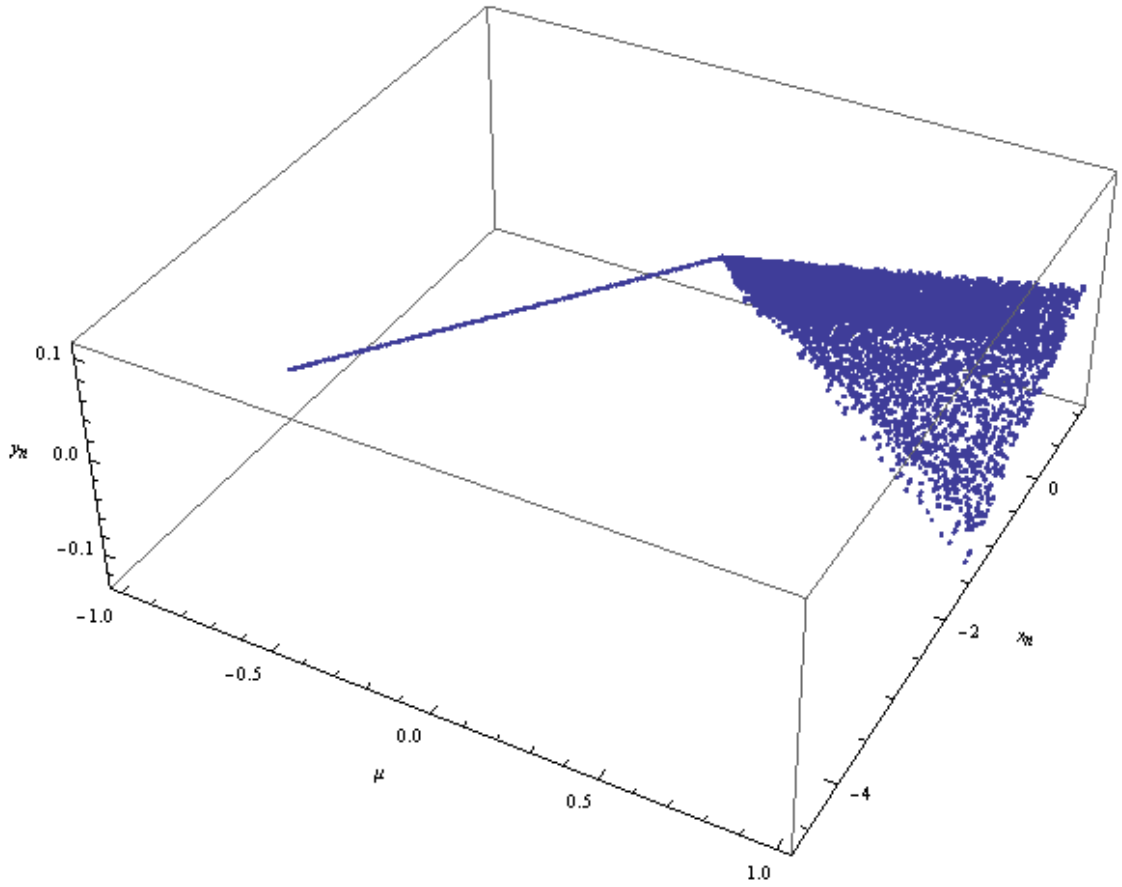

Figure 23 This bifurcation diagram occurs when $\tau_L = 0.5534, \tau_R = -5.4934, \delta_L = -0.02825$, and $\delta_R = -0.25165$. As expected, when conditions (4.29) and (4.30) are not met, we result in chaos.

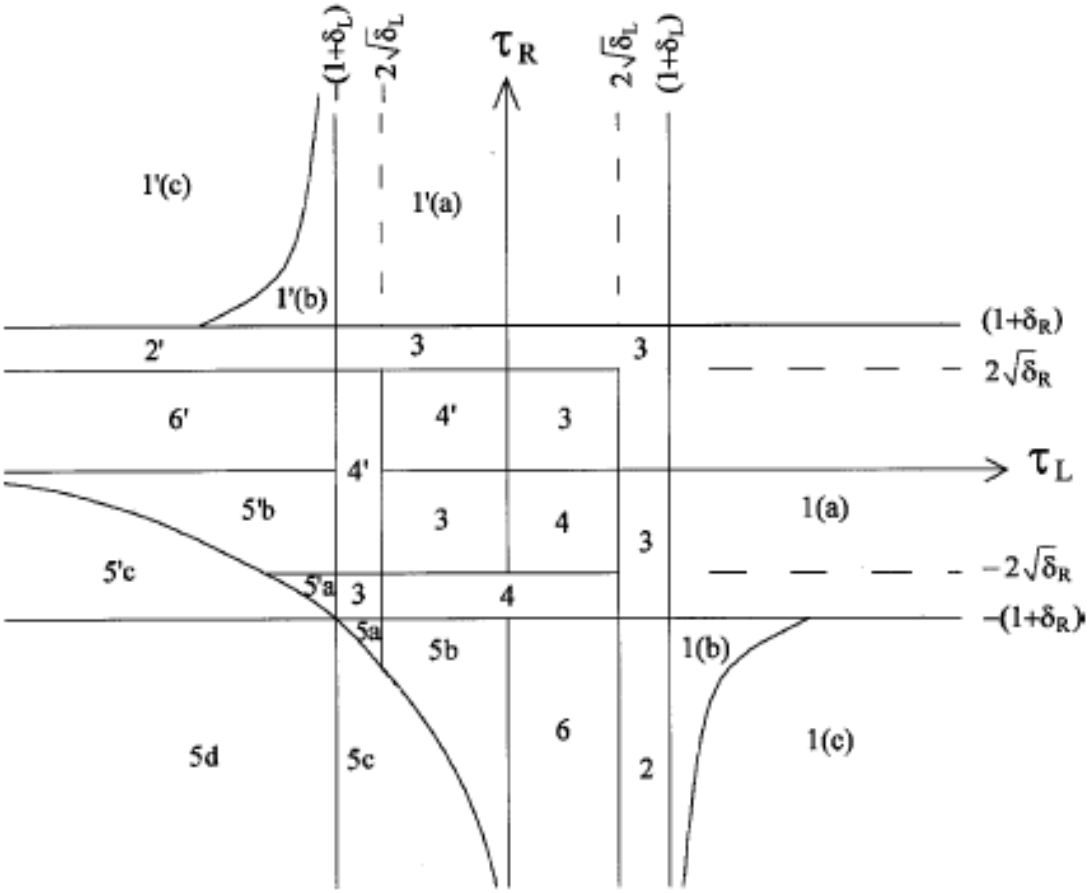

Figure 24 This figure shows the parameter map for the two-dimensional piecewise linear system of equations with positive determinants; copied from Banerjee et al. [27].

$$-1.4878 = -2\sqrt{\delta_R} < \tau_R < 0$$

must hold. We define $\tau_L = 1.1$ and $\tau_R = -0.0534$ to satisfy these conditions. We see the result in Figure 25A, which indeed shows no attractor leading to a period-1 attractor.

The next result that we hope to obtain is shown in region 1c in Figure 24. We expect this region to produce no attractor leading to a chaotic attractor. We see, then, that the following should hold:

$$1.02825 = 1 + \delta_L < \tau_L$$

and

$$\tau_R < -(1 + \delta_R) = -1.55165.$$

We define $\tau_L = 1.1$ and $\tau_R = -5.534$ to satisfy these conditions. We see the result in Figure 25B, which indeed shows no attractor leading to a chaotic attractor.

Another result that we can obtain is shown in region 2 in Figure 24. We expect this region to produce a period-1 attractor leading to a chaotic attractor. We see, then, that the following should hold:

$$0.3362 = 2\sqrt{\delta_L} < \tau_L < 1 + \delta_L = 1.02825$$

and

$$\tau_R < -(1 + \delta_R) = -1.55165$$

We define $\tau_L = 0.9534$ and $\tau_R = -1.9534$ to satisfy these conditions. We see the result in Figure 25C, showing a period-1 attractor leading to a chaotic attractor.

Lastly, we want to obtain the results shown in region 3 in Figure 24. We expect this region to produce a period-1 attractor leading to a period-1 attractor. We know that the following should hold:

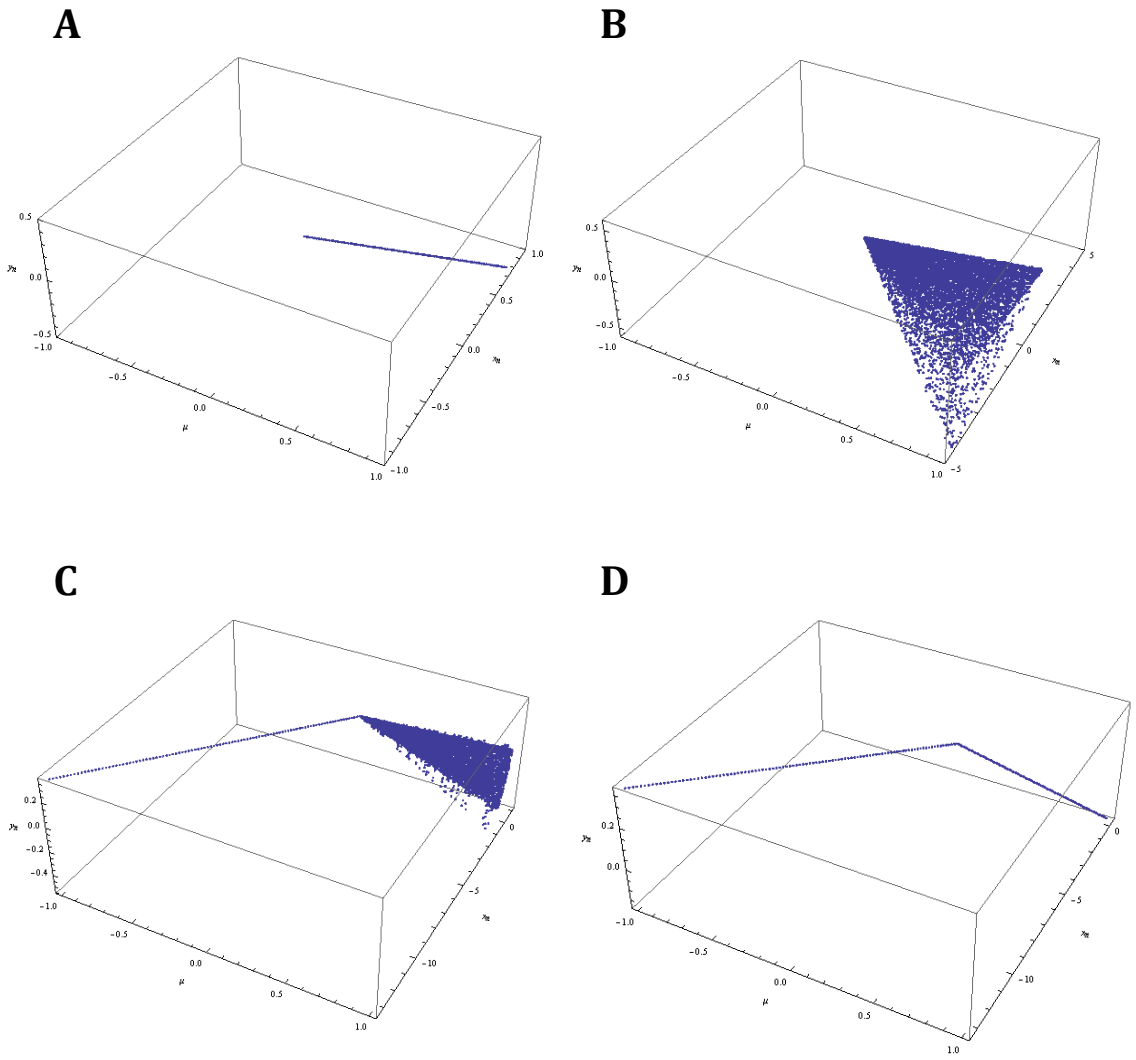

Figure 25 For these figures, we defined positive determinants, given by Equation (4.33), so that $\delta_L = 0.02825$ and $\delta_R = 0.55165$. Then we define different trace values for each situation. (A) $\tau_L = 1.1, \tau_R = -0.0534$; (B) $\tau_L = 1.1;\ \tau_R = -5.534$; (C) $\tau_L = 0.9534;\ \tau_R = -1.9534$; (D) $\tau_L = 0.9534;\ \tau_R = -1.4934$.

$$0.3362 = 2\sqrt{\delta_L} < \tau_L < 1 + \delta_L = 1.02825$$

and

$$-1.55165 = -(1 + \delta_R) < \tau_R < (1 + \delta_R) = 1.55165$$

We define $\tau_L = 0.9534$ and $\tau_R = -1.4934$ to satisfy these conditions. We see the result in Figure 25D, showing a period-1 attractor leading to a chaotic attractor, as expected. With Figure 25, we have provided several examples in support of their theoretical analysis.

CHAPTER V

SUMMARY AND CONCLUSION

In this thesis, we have developed mathematical models to describe calcium cycling within a cardiac cell. The ability to simulate calcium cycling is significant in the relevance of predicting alternans, which would ultimately assist in preventing sudden cardiac arrest, one of the leading causes of death in the United States. Alternans triggers arrhythmias such as ventricular fibrillation within the heart, and is a harbinger for sudden cardiac arrest.

In Chapter 3, a one-dimensional mapping model was developed based on the simplified assumption that the total calcium concentration within the cell is constant. Thus, the model describes the regulation of the peak cytoplasmic calcium in one heartbeat as a function of that in the previous beat. We then explored the bifurcation patterns of the developed mapping model using the outcomes in Yorke et al. [24]. This model provided us with some interesting results about the wide range of bifurcations that might occur when increasing the pacing period of our one-dimensional linear mapping model.

In Chapter 4, a two-dimensional mapping model was developed, which allows variation of the total calcium concentration within the cell. The modeling scheme was adopted from Qu et al. [3]. State variables of the model include the calcium load in the sarcoplasmic reticulum at the end of each beat as well as the total cellular calcium at the end of each beat. In order to investigate border-collision bifurcations, we carried out a piecewise linear approximation of the model in Qu et al. [3]. Numerical results showed

that the piecewise linear functions approximate the original functions well. We then transformed the two-dimensional piecewise linear model into the normal form outlined in Banerjee and Grebogi [27]. Bifurcation patterns in the two-dimensional model were explored to show that there exists a plethora of possible instabilities in calcium cycling. This information might encourage us to study the eigenvalues of continuous maps at the bifurcation point for both calcium cycling models and those describing voltage dynamics, as other recent research suggests [28-29].

There are a few modifications, which we would like to suggest for future research. First, the second model would be much more reliable if we had not performed the linear approximations to experimental data. Studying the original system of equations, we could have used affine approximations near the threshold and studied bifurcation phenomenon that occurred locally. This could have provided much more realistic information regarding the onset of alternans based on calcium cycling in a cardiac cell.

Another modification that could be made to the two-dimensional model is to propose an even more complex model, relying on more than the generalized processes that were described in this thesis. Calcium flow in a cardiac cell is much more complicated than simply measuring the total cellular calcium and the amount of calcium within the SR at the end of a beat. There are L-type calcium channels that open at the voltage stimulation, allowing calcium to flow into the cell, as well as sodium-calcium exchanges and ATPases which have a great deal to do with the amount of calcium in the cytoplasm at a given time. Rather than including these processes individually, our model generalizes calcium flowing into and out of the cell by only observing the difference in

total cellular calcium between beats, and even this value is only dependent on the length of the pacing period. There is clearly much more going on inside of the cell which is not represented in these simplified models.

A final modification, which we would like to suggest for both of these models, is the dependence on APD. Although we are observing the onset of arrhythmias at sufficiently fast pacing periods, we are not observing the dependence of this calcium cycling on the voltage dynamics of the cell. Research suggests that the voltage dynamics of a cardiac cell are dependent on the ionic flow within the cell. Thus, we should expect that bifurcation diagrams involving APD will be directly related to the results of these calcium cycling models.

The goal of this thesis was to observe border-collision bifurcations in calcium cycling models. The results that were obtained from both of these models suggest that, while alternans is the main focus of current research, there may in fact be a wide range of arrhythmias that can occur in the heart before the onset of sudden cardiac arrest. Additional experimental analysis is required to either confirm or deny the bifurcation phenomenon observed in this thesis.

REFERENCES

[1] Mozaffarian D, Benjamin EJ, Go AS, et al. Heart disease and stroke statistics—2015 update: a report from the American Heart Association. Circulation. 131: E29-322. 2015.

[2] Keener, J. and Sneyd J. Mathematical Physiology II: Systems Physiology. Springer. 2nd Edition. 2009.

[3] Qu, Z., Shiferaw Y. and Weiss, J. Nonlinear dynamics of cardiac excitation-contraction coupling: An iterated map study. Physical Review E 75, 011927. 2007.

[4] Cain, J. W. Taking math to heart: Mathematical challenges in cardiac electrophysiology. Notices of the AMS. Vol. 58, No. 4.

[5] Hodgkin, A. L. and Huxley, A. F. A quantitative description of membrane current and its application to conduction and excitation in nerve, J. Physiol. London 117. 1952. 500-544.

[6] Zhao, X. Indeterminacy of spatiotemporal cardiac alternans, Physical Review. E 78:011902. 2008.

[7] J. N. Weiss, Z. Qu, P. S. Chen et al., Circulation. 112, 1232. 2005.

[8] Z. Qu and J. N. Weiss, J. Cardiovasc. Electrophysiol. 17, 1042. 2006.

[9] Strydom, N.B. et al. Journal of Applied Physiology. 25, 191. 1968.

[10] Panfilov, A. Chaos. 8, 57. 1998.

[11] Pastore, J. M. et al. Circulation. 99, 1385. 1999.

[12] Bloomfield, D. M. et al. Journal of American Coll. Cardiology. 47, 456. 2006.

[13] Shusterman, V., Goldberg, A., London, B. Circulation. 113, 2880. 2006.

[14] Karma, A. Chaos. 4, 461. 1994.

[15] Garfinkel, Y. H. et al. Proc. Natl. Acad. Sci. USA. 97, 6061. 2000.

[16] Bers, D. Cardiac excitation-contraction coupling. Nature. Vol 415. 2002.

[17] Bootman, M.D., Berridge, M.J. and Roderick, H.L. Calcium signalling: more messengers, more channels, more complexity. Current Biology. 12, R563–R565. 2002.

[18] Tolkacheva, E. G. and Zhao, X. Nonlinear dynamics of periodically paced cardiac tissue. Nonlinear Dynamics. 68: 347-363. 2012.

[19] Schaeffer, D. G. et al. An ionically based mapping model with memory for cardiac restitution. Bull. Math. Bio. 69. 459-482. 2007.

[20] Franz, M. et al. Electrical and mechanical restitution of the human heart at different rates of stimulation. Circulation Research. 53, 815. 1983.

[21] Goldhaber, J. et al. Action potential duration restitution and alternans in rabbit ventricular myocytes. Circulation Research. 96, 459. 2005.

[22] T. R. Shannon, K. S. Ginsburg, and D. M. Bers, Biophysical Journal. 78, 334. 2000.

[23] E. A. Sobie, L. S. Song, and W. J. Lederer, J. Cardiovascular Electrophysiology. 17, S64. 2006.

[24] J. A. Yorke and H. E. Nusse. Border-collision bifurcations for piecewise smooth one-dimensional maps. Int. J. Bifurcation Chaos. 05, 189. 1995.

[25] Y. L. Maistrenko, V. L. Maistrenko, and L. O. Chua. Cycles of chaotic intervals in a time-delayed Chua's circuit. Int. J. Bifurcation Chaos. 3, 1573. 1993.

[26] F. Takens. Transitions from periodic to strange attractors in constrained equations. Dynamical Systems and Bifurcation Theory. 160, 399. 1987.

[27] S. Banerjee and C. Grebogi, Border collision bifurcations in two-dimensional piecewise smooth maps. Physical Review. 59, 4. 1999.

[28] A. Petrie and X. Zhao. Estimating eigenvalues of dynamical systems from time series with applications to predicting cardiac alternans. Royal Society. 468, 3649. 2012.

[29] W. Groenendaal, F. A. Ortega, T. Krogh-Madsen, and D. J. Christini. Voltage and calcium dynamics both underlie cellular alternans in cardiac myocytes. Biophysical Journal. 106, 2222. 2014.

VITA

Jacob Michael Kahle was born and raised in Huntingburg, Indiana. Upon graduating from high school in 2007, he went on to further his education at the University of Evansville, where he graduated Magna cum Laude in 2011 with a Bachelor of Arts in Mathematics. Upon graduation, he applied and was accepted at Oakland City University, where he completed the Master of Arts in Teaching degree in 2012. Jacob continued his education at the University of Tennessee, Knoxville, where he pursued a Master of Science in Mathematics. During his time at the university, he worked as a Graduate Teaching Assistant in the Student Success Center as an academic coach, as well as a supplemental instruction and tutoring coordinator. Upon graduation, he plans to put his new degree and education to work both in the classroom and in industry.